L-462

ARR Jan. 1942

NATIONAL ADVISORY COMMITTEE FOR AERONAUTICS

WARTIME REPORT

ORIGINALLY ISSUED
January 1942 as
Advance Restricted Report

INVESTIGATION OF DRAG AND PRESSURE DISTRIBUTION OF WINDSHIELDS AT HIGH SPEEDS

By James B. Delano and Ray H. Wright

Langley Memorial Aeronautical Laboratory
Langley Field, Va.

CASE FILE
COPY

WASHINGTON

NACA WARTIME REPORTS are reprints of papers originally issued to provide rapid distribution of advance research results to an authorized group requiring them for the war effort. They were previously held under a security status but are now unclassified. Some of these reports were not technically edited. All have been reproduced without change in order to expedite general distribution.

INVESTIGATION OF DRAG AND PRESSURE DISTRIBUTION OF WINDSHIELDS AT HIGH SPEEDS

By James B. Delano and Ray H. Wright

SUMMARY

Tests were conducted in the NACA 8-foot high-speed wind tunnel to determine the loads and the load distributions at high speeds for a number of windshields of the cockpit-canopy type. Drag data were obtained simultaneously with the load data. Ten windshields of various designs similar to those in general use were included in these tests. A new windshield designed to give low local loads and low drags was also tested. These windshields were mounted on a DC-3 fuselage and wing model. Pressure distributions were obtained for the wing alone and for the fuselage mounted on the wing. From the pressure data an analysis was made of the interference effects between a windshield and the model. The tests were made at Mach numbers ranging from 0.12 to 0.71, and a study of the effects of compressibility on loads and drags was thereby permitted.

The load and drag data obtained in these tests are presented graphically. The pressure coefficients are presented at a wing angle of attack of -0.67 (lift coefficient = 0.10) for Mach numbers ranging from 0.19 to 0.71 and at wing angles of attack up to 6° (lift coefficient = 0.82) for a Mach number of 0.19. Windshield drag coefficients are plotted against Mach number at wing angles of attack of -0.67° and -1.55° and against wing angle of attack at a Mach number of 0.19.

The results of these tests show that both the local loads and the drags vary greatly among different windshields. The drag of a good windshield was found to be small, only about 2 percent of the drag of a good airplane; but the drag of a bad windshield might easily be ten times as great. Blunt noses and blunt tails or sharp corners transverse to the flow were generally found to be responsible for both high drags and high local loads. Windshields having high drags also had high local loads; some of the windshields having low drags had moderately high local loads. Low local loads are favored by large fineness ratios and by shapes that tend to distribute the load uniformly over the main body of the windshield. For the bad windshields the drags and for the good windshields the local loads increased greatly with increase in Mach number.

Interference from the wing and fuselage is shown to have an important effect on the windshield and usually serves to increase the loads. Predictions of loads at high speeds made from low-speed data may be greatly in error unless the effect of both compressibility and wing interference is taken into account. The new windshield, designated the X-2 windshield, was found to have both low drag and low local loads.

INTRODUCTION

The windshield or cockpit canopy is designed to provide head room, vision, and protection to occupants of the cockpit of a pursuit or a similar type of airplane. The disturbance to the flow over the fuselage should, of course, be a minimum. The increase in drag due to the cockpit enclosure should be as small as possible and, in order that sufficient strength may be provided, the loads should be small and of known magnitude and distribution. It is especially important that the high loads attained at high speeds be known with a reasonable degree of accuracy. The entire cockpit enclosure, including the nose or windshield proper, the middle piece or hood, and the tail, will be referred to in this report as the "windshield."

Most of the windshield data in existence up to the time of the present investigation had been obtained at low speeds. Low-speed drag data had been obtained in the investigations described in references 1 and 2; whereas other windshield investigations had been concerned mainly with the field of view and the adaptability of windshields to bad weather (references 3 and 4). Undoubtedly much low-speed load data had been obtained by manufacturers, but this work is generally unavailable. No high-speed load data had been obtained. The only high-speed windshield data available were the results reported in reference 5, and that investigation was limited to finding the effect of various geometrical factors, such as nose shape, nose length, tail shape, tail length, and others on the drag of windshields. The failure of several windshields in high-speed dives served to emphasize the necessity of obtaining information on the magnitude and distribution of loads at high speeds.

This investigation was conducted primarily to obtain high-speed load data, including the effect of compressibility on loads for a number of representative windshield shapes. Secondary considerations included determination of the critical speeds of the windshields, measurement of the windshield drags for comparison with those obtained in reference 5, and study of the flow over the windshield-fuselage-wing combination for correlation with the drag and load data. A short discussion of the rather large mutual-interference effects between wing and windshield and between the wing-fuselage combination and the windshield is given in an appendix.

These tests included drag and pressure measurements, covering a speed range roughly from 100 to 500 miles per hour on several of the windshield combinations of reference 5 and on two windshields of more advanced design. For use in the flow and interference study, pressures about the wing and fuselage were also measured. This work in conjunction with reference 5 gives comprehensive drag and load data from which drags and loads for most commonly used windshields can be reliably estimated.

APPARATUS AND METHOD

This investigation was made in the NACA 8-foot high-speed wind tunnel, which is described briefly in reference 6. The basic model on which the windshields were mounted was a 1/8-scale model of the DC-3 airplane used in previous tests (reference 5). The inboard panel of the wing employs the NACA 2215 section. Engine nacelles, landing gear, tail wheel, and tail surfaces were omitted in these tests and the discontinuity at the cabin was completely faired out so that drag changes relative to the drag of the basic model might be as large as possible.

The 11 windshields shown in figure 1 were used in this investigation; nine of these were used in previous windshield tests (reference 5) and are based on simple geometric shapes. The remaining two, the X-1 and the X-2, are of a later and more advanced design. For purposes of comparison all the windshields were designed to have a maximum cross-sectional area of approximately 0.152 square foot. Table I with figure 1 gives the ordinates for the component parts N, M, and T for the first nine windshields shown in figure 1. These letters refer to the nose, middle, and tail pieces, respectively, the combination being designated by three numbers in the same order. The symbol 0, as in the combination 4-0-3, indicates that the middle piece M has been omitted and that the nose piece N and the tail piece T butt against each other. Figures 2 and 3 give the ordinates for the X-1 and the X-2 windshields, and figure 4 show the X-2 mounted on the fuselage. Both the X-1 and the X-2 windshields are characterized by two basic airfoil sections; the X-1 has straight-line elements connecting these sections in a transverse vertical plane and the X-2 has straight-line elements connecting equal percentages of chord on the two basic airfoil sections. The top part of both windshields is rounded to parabolic sections in transverse vertical planes.

The location of the windshields on the fuselage is shown in figure 5. The beginning of the tail piece came in the same position, about 39.69 inches from the nose of the fuselage for all the windshields. The windshields were all so located, similarly with respect to the flow over the fuselage, that the results are practically comparable. The direction of the axes of the windshields coincided with that of the fuselage axis, which made an angle of -2° with the chord of the wing.

Pressure orifices were installed on only one side of the windshield, the wing, and the fuselage. Figure 1 shows the location of lines along which orifices were located on the windshields. These lines are designated by numbers that agree with the numbers shown in the pressure-distribution plots presented later. No attempt was made to give the location of all the individual orifices on the windshields. These locations can be determined from the pressure plots where pressure coefficients at each orifice are plotted. The location of the orifices on the wing and fuselage is shown in figure 6.

The set-up of the model in the tunnel is shown in figure 7. The pressure lines were installed completely inside the model, running out of the tunnel at the wing tips. They were connected to a multiple-tube manometer filled with tetrabromethane. A camera was used to record the liquid levels in the manometer.

The force and the pressure data were taken simultaneously; the drags obtained therefore exactly correspond to the pressure data. Since the windshield drags were small in comparison with the drag of the entire model, it was necessary to assure that the model drag remain nearly constant between runs. In order to minimize any error due to fluctuation of the transition point, transition was fixed on the model by means of 1/4-inch transition strips placed at $17\frac{1}{2}$-percent chord on the upper surface and at 6-percent chord from the leading edge on the lower surface of the wing and in a ring around the fuselage at 12 inches from the fuselage nose. Except for the strips to fix the transition location, the surfaces of the model were maintained aerodynamically smooth. The drag caused by the windshield was determined by taking the difference between the drag of the model wth well-faired windshield and a basic drag obtained for the wing and fuselage alone. Two later additional basic-drag runs checked well with the original.

These tests included lift, drag, pitching moment, and pressure-distribution measurements for the wing and fuselage alone and in combination with the 11 windshields. The Mach number ranged from 0.12 to 0.71, corresponding to a Reynolds number range from 1,300,000 to 5,300,000 based on the mean aerodynamic chord of 17.3 inches. Lift, drag, and pressure measurements were made at a Mach number value of approximately 0.19 for a range of lift coefficients from approximately -0.2 to 0.8, corresponding to angles of attack from -3.5° to 6°. The lift-coefficient range was limited at high speeds by the strength of the wing. Most complete data were obtained for a lift coefficient of 0.10, corresponding to an angle of attack of -0.67°.

PRECISION

Systematic errors affecting the windshield drag and the pressure measurements arise principally from buoyancy and constriction effects. The results for comparative purposes, however, are unaffected to any important degree because the sizes of all configurations tested are practically the same. The absolute values, on the other hand, tend to be somewhat less than the values presented. These errors are small and at a Mach number of 0.65 are believed to be not greater than 5 percent on the dynamic pressure and 4 percent on the Mach number. At lower speeds the errors are much smaller.

Accidental errors affecting the drag results to any important degree may be present at the lowest speeds and at the highest speeds after compression shock is formed. At the lowest speeds these errors occur because of the difficulty of measuring the very low loads and are greatest for the best windshields. At the highest speeds when compression shock is formed on the wing, these errors occur because of the unsteady nature of the flow and because of the difficulty of determining drag increments where the slopes of the drag curves are extremely steep, that is, in the region where the drag curves are rising almost vertically beyond the critical speed of the wing.

RESULTS

In the presentation and the analyses of the results of this investigation the following symbols are used:

p_s static pressure in air stream

p_l	local static pressure on model surface
ρ	mass density of air stream
V	true air-stream velocity
q	dynamic pressure $(1/2\rho V^2)$
a	speed of sound in air stream
M	Mach number (V/a)
M_{cr}	Mach number corresponding to attainment of local speed of sound
P	pressure coefficient $\left(\frac{p_l - p_s}{q}\right)$
P_i	low-speed pressure coefficient
P_{cr}	pressure coefficient corresponding to attainment of local speed of sound
C_D	drag coefficient of model based on wing area
C_L	lift coefficient
$C_{m_{c/4}}$	pitching-moment coefficient at quarter chord
α	angle of attack of wing
ΔD_w	difference between drag of model with and without windshield at same angle of attack and Mach number
F_w	maximum cross-sectional area of windshield
$C_{D_{F_w}}$	drag coefficient of windshield $\left(\frac{\Delta D_w}{qF_w}\right)$
ΔV	velocity increment or induced velocity
$\Delta V/V$	velocity-increment coefficient
v	local velocity $(V + \Delta V)$
γ	ratio of specific heats c_p/c_v for air

The method of determining the dynamic pressure q, the Mach number M, and the Reynolds number are described in reference 7. The symbols C_L, C_D, and $C_{m_{c/4}}$ represent the usual nondimensional coefficients with the pitching moment taken about the quarter-chord point. Pressure coefficients were calculated from the photographic records of the pressure differences and the dynamic pressures measured on the multiple-tube manometer.

The presented data are plotted against the predominating parameter, the Mach number. The Reynolds numbers are shown for the corresponding Mach numbers of these tests in figure 8. Figure 9 shows the lift coefficient of the model plotted against angle of attack α of the wing and figure 10, the lift coefficient against Mach number. The data presented herein apply only to smooth windshields mounted in the particular location relative to the particular wing and fuselage used in these tests and in the absence of propeller slipstream. In the application of the data to design problems, therefore, departures from these conditions should be kept in mind.

The windshield drag coefficients $C_{D_{F_W}}$ for the 11 windshields are plotted against angle of attack α of the wing for $M = 0.193$ in figure 11 and against M for $\alpha = -0.67^\circ$ and -1.55° in figure 12. The windshield forms corresponding to the various drag curves are indicated on the figures. These curves show drags generally increasing with angle of attack and with Mach number. The drag values diverge widely among different windshields. The reasons for these variations will presently be discussed in detail.

The effect of different types of windshield on the moment is shown in figure 13 where $C_{m_{c/4}}$ for three different windshields and for the model without windshield is shown plotted against M. The windshields increase the absolute value of the pitching-moment coefficient, which is negative. The effect is small at low speeds but increases with Mach number. It is evidently due to the fact that higher negative pressures act over the windshield than exist on the fuselage in this region without the windshield. The pressures add a negative moment much greater than the positive moment produced by the drag. With the three windshields shown, the pitching-moment coefficients are about the same up to a Mach number of 0.60. For Mach numbers greater than 0.60 the 7-3-4 windshield, which has the highest drag and also the highest negative pressure peak, also gives the greatest increase in negative moment. The change in moment for any given windshield installation evidently must depend on its position.

The pressure-distribution data for the 11 windshields are presented as pressure coefficient P plotted against distance in inches, measured along the longitudinal axis, from the foremost point of the windshield.* Figures 14 to 24 give pressure distributions at $\alpha = -0.67^\circ$ for six values of M from 0.197 to 0.710. The approximate locations of the orifice lines on the models and the symbols representing them are shown on the plot. In order to avoid confusion, only points in the orifice line having the highest negative pressure coefficient are connected. The peak negative pressures are seen to be widely different for different windshields; in most cases, they increase rapidly with Mach number. The pressure coefficients corresponding to the attainment of the local speed of sound are indicated as P_{cr}. Pressure coefficients for several angles of attack up to 6° are plotted for eight windshields in figures 25 to 32. These data were taken at a Mach number of approximately 0.192, except in the case of the 10-1-2 windshield for which the Mach number is 0.339. A separate plot is shown for every orifice line, the symbols in this case indicating the wing angle of attack. As might have been expected, negative pressures increase with increase in angle of attack, an effect due at least partly to wing interference, as shown in the appendix. The peak negative pressure coefficients for the 11 windshields are shown plotted against M in figure 33. The point at which the peak negative-pressure curve intersects the curve marked P_{cr} determines the critical Mach number M_{cr} of the windshield in combination with the wing and the fuselage. The critical speeds are evidently considerably different for different windshields. The windshield pressure data are discussed in detail in the section of this report on loads.

DISCUSSION

Drag.- From figures 11 and 12 the drag coefficient of a good windshield, based on the cross-sectional area, is seen to be about 0.035. For a usual ratio of windshield cross-sectional area to wing area, this value corresponds to about 2 percent of the drag of a good airplane. The drag of a bad windshield may be 10 times this value or 20 percent of the airplane drag.

In order to gain some idea of the approximate magnitude of the drag that should be expected on a windshield, a rough estimate was made of the skin-friction drag that was added when the 2-0-3 windshield was installed. This estimate showed a windshield drag coefficient of 0.026 for wholly turbulent flow or 0.020 with laminar flow over the forward 18 percent of the windshield. It is evident that measured drags substantially higher than these values must have been largely pressure drag, such as would be obtained with flow separation. Severe separation should, in fact, be expected for forms such as the 6-1-2, the 9-1-2, the 7-3-4, and the 8-4-5 windshields, which have short noses terminating at sharp corners transverse to the flow. Figures 18, 19, 21, and 22 show that these windshields have high, sharp negative pressure peaks just back of the corners. These peaks are followed by large positive pressure gradients conducive to separation of the flow. For the 10-1-2 windshield the separation is less severe because the nose is longer and less blunt; but at high Mach numbers, because of the steepening of the pressure gradients (fig. 20), the separation becomes pronounced. The 3-1-1 windshield has a long nose without the sharp edge, but it has too short and too blunt a a tail. Figure 16 shows the resulting rear pressure peak and the following steep positive pressure gradient. The flow separates in this region because the kinetic energy in this boundary-layer air is insufficient to overcome the gradient. The separation region is smaller, however, and the consequent drag increase less than for those windshields for which the flow separates near the nose. The effect of increase in angle of attack is somewhat similar to that of increase in Mach number in increasing separation. (See fig. 11.) This increased separation occurs because, as seen in figures 25 to 32, the pressure gradients increase with angle of attack, though at least part of the effect is probably due to interference from the wing. (See the appendix.)

---

*In figures 14 to 32 the distance scale was originally intended to apply to the sketch of the windshield as well as to the pressure distribution. The windshields are drawn to this distance scale and therefore should be shifted so that the nose of the windshield is placed at zero.

A glance at figure 12(a) in conjunction with figures 1, 2, and 3 will show that the windshields having low drag are characterized by long noses and, especially, long tails and by the absence of sharp corners transverse to the flow. Reference 5 shows that the radius of curvature of the surface on the shoulder between the nose and middle pieces of a windshield should be not less than one-fourth of the windshield height. Figures 14, 15, 17, 23, and 24 show further that these windshields are characterized by the absence of high, sharp negative pressure peaks and by low positive pressure gradients over the tail. Of the windshields represented in figure 11, the same ones, except for the 4-0-3, show low drag throughout the angle-of-attack range that show low drag at $\alpha = -0.67^\circ$. The bad windshields become worse as the angle of attack is increased. For the 4-0-3 windshield at the highest angle, 6°, some separation has probably developed around the tail in the windshield-fuselage juncture.

The effect of compressibility is to increase the drags, particularly of the windshields having high drag already, because for these windshields the flow is separated and compressibility increases the severity of separation; and because also, except for the 3-1-1 windshield they have high peak negative pressures and therefore low critical speeds. A comparison of figure 12(a) with figure 33 shows, however, that as the Mach number is increased large increases in drag occur before the critical speed is reached, indication being thus given that the increased severity of separation may be the primary cause of the drag increase.

An interesting case parallel to a condition that has sometimes been found for wings is that of the 10-1-2 windshield. Up to a Mach number of about 0.50 this windshield shows a low drag, indicating little separation; but at this Mach number, which is far below the critical value indicated in figure 33, the drag suddenly begins to increase. The probable explanation is that even at low speeds the flow is on the verge of separating just back of the nose. Only the increase in pressure gradient produced by increase in Mach number is required to induce complete separation with consequent large increase in drag.

Separation may be expected to reduce the peak negative pressures and, therefore, to increase the critical speed as indicated for the bad windshields, 7-3-4, 9-1-2, 8-4-5, 6-1-2, 10-1-2, and 3-1-1 in figure 33, where it is seen that for three of the windshields having the highest drags the peak negative pressures actually decrease with Mach number, but the drag of the bad windshields is already so high that in respect to drag the critical speed has little meaning.

For the five good windshields, the 3-1-2, the 2-0-3, the 4-0-3, the X-1, and the X-2, the negative pressure peaks increase very rapidly with Mach number, but even with the interference (see appendix) the critical Mach numbers of the best of these are well above $M_{cr} = 0.70$, which is as high as that of any wing with which they are likely to be used. The turning up of the drag curves around $M = 0.65$ does not indicate the critical speeds of these windshields, and this drag increase is probably not due to any characteristic of the windshields themselves. Instead, it is probably due to interference of the windshield on the wing, whereby the apparent critical speed of the wing is shifted to a lower stream Mach number. The sharp increase in wing drag that occurs at the critical speed then comes at a lower stream Mach number with the windshield in place than without and, when the two corresponding drag curves are compared at equal stream Mach numbers, the difference in drag above the wing critical Mach number, about 0.61 with fuselage, may be very great. As is pointed out in the appendix, the windshield interference will affect the wing over only a limited region; but, if only half of the estimated possible 2-percent lowering of the apparent critical speed is assumed, the effect, even if operative over only a small portion of the wing, is quite sufficient to explain the observed turning up of the windshield drag curves. Because of the steepness of the drag curves in this region, a similar effect, operating either to reduce or to increase the apparent windshield drag coefficient, may be produced by any small error in determining the stream Mach number. The general unreliability of the drag curves above the wing critical speed already has been commented upon. Actually, the real drag of the windshield is better indicated by the values for Mach numbers below the wing critical speed, and the critical speed of the windshield itself, as well as the speed at which the drag of the windshield itself may rise rapidly, is given in better approximation as the speed at which the curve of peak negative pressure against Mach number intersects the critical-pressure curve.

Loads.- Figures 14 to 32 show that the local loads on different windshields varied greatly and in certain cases were extremely high. The loads on the side, closer to the fuselage and wing, were generally slightly higher than those on the top. A consideration of the interference (see the appendix) indicates that this result might be expected. Although the actual magnitude of the loads was influenced by interference, relative values were probably little affected, because the interference must have been the same for different tests and also did not vary much along the windshield length. As might have been expected, both from a consideration of the windshield shapes and of the interference effect, the loads increased with angle of attack (figs. 25 to 32).

The pressure-distribution curves fell generally into three classes: distributions with a single peak as illustrated by the 2-0-3 windshield (fig. 14), distributions with two peaks as the 3-1-1 windshield in figure 16, and approximately flat distributions as shown in figures 15 and 24 for the 4-0-3 and the X-2 windshields, respectively. In general, where stream static pressure inside the windshield was assumed, the forces were such as to tend to pull the canopy off and to push the nose in.

Examination of figures 14 to 24 shows that the windshields having high local loads are characterized by short noses, short tails, or sharp corners. The highest peak negative pressures occurred behind sharp corners transverse to the flow. Other factors that tend to increase loads are interference, compressibility (to be discussed presently), and low fineness ratio. The effects of interference and low fineness ratio are similar in that both tend to produce higher total loads but only small changes in the distribution. Thus, in order to avoid high total loads, the interference should be made small, as by using a thin wing, and as thin a windshield should be used as is consistent with space requirements. In addition, local loads may be reduced by using well-rounded shapes similar to the 2-0-3 and the X-1 windshields (figs. 14 and 23) and, finally, by using better forms designed for approximately flat pressure distributions, such as the 4-0-3 and the X-2 windshields (figs. 15 and 24). The possibility of taking advantage of favorable interference is discussed in the appendix.

The relation between large positive pressure gradients and separation, with consequent large drag increase, already has been pointed out. Because these large positive pressure gradients followed high negative pressure peaks, the windshields having high drag also had high local loads (figs. 12, 16, 18 to 22). If separation does not occur, the drag will be low even if the negative pressure peaks are high, though possibly not so low as though the negative pressures were better distributed. This condition existed for the 2-0-3 and X-1 windshields (figs. 14 and 23), which had moderately high negative pressure peaks but low drags. If for the high-drag windshields the flow had followed the surface instead of separating from it, the drag would have been greatly decreased, but the local loads would have been much higher. Thus, separation, which causes the high drags, tends to reduce the local loads. The effect of separation at the sharp corners is to cause the flow to follow a path having a large radius of curvature. The curvature here largely determines the negative-pressure coefficient. If the sharp corner is replaced by a small radius of curvature, the peak negative-pressure coefficient will not be much affected until a radius equal to that followed by the separated flow is reached; consequently, for equal changes in flow direction, the peak should be, up to a moderate value of the radius of curvature at the surface, not much different from those measured. In reference 5 it was found that considerable drag increases occurred with radii of curvature less than about 25 percent of the windshield height. This result indicates separation, and it may therefore be deduced that this value is approximately the corner radius below which the pressure data obtained for the windshields having sharp edges apply. Radii of curvature larger than this value are probably needed to reduce the local loads.

The two windshields having the lowest peak negative pressures also showed low drags (figs. 12, 15, and 24). This result may not always be the case, because a windshield having too blunt a tail and, therefore, high drags might also have fairly low loads.

The effect of compressibility on the loads may be seen from figures 14 to 24. In every case for which separation (as indicated by high drag) did not occur, the negative-pressure coefficients increased markedly and continuously with Mach number. The peaks increased more rapidly than the general pressures, thereby increasing the concentrated loads, a circumstance favorable to local failure. The increase amounted to as much as 100 percent between $M = 0.20$ and $M = 0.70$. In cases for which separation occurred, the peaks did not always increase with Mach number, but they broadened out and the general negative pressures increased with the result that the total loads were increased. The effect of compressibility in increasing the pressure gradients, thus inducing separation with consequent drag increase, has already been discussed.

At speeds above the critical value (crtical pressure coefficient indicated by P_{cr}), the peaks show a general broadening, usually accompanied by an increase in peak negative-pressure coefficient, as expected from two-dimensional investigations. (See figs. 14, 18 to 22.) This result means that, as the Mach number is increased beyond the critical value, a considerable increase in loads - both local and total - occurs.

The increase in peak negative pressure with Mach number, shown in figure 33, was more rapid for the windshields for which separation did not occur. Part of this increase was due, as shown in the appendix, to interference from the wing and fuselage. The increase was much more rapid than that given by the factor $1/\sqrt{1 - M^2}$. This fact should be kept in mind when attempting to estimate loads at high speeds from low-speed data. The critical speed was not attained in these tests for those windshields having the lowest peak negative pressures (figs. 15, 17, and 24), and the effect of compressibility on these windshields was less. At higher Mach numbers these windshields would probably show the same effects that the other windshields showed at the Mach numbers of these tests.

Design considerations.- The designer will be confronted with a number of considerations in designing a windshield that meets the use requirements and is, at the same time, aerodynamically permissible. One of the important considerations is strength. From the results of these tests, it is apparent that local loads vary greatly among different windshields and that these loads increase rapidly with speed, high local loads increasing more rapidly than low local loads. These loads and their increase with Mach number must be allowed for in design, particularly if the airplane is to be used in a dive where the windshield, the wing, or both may be operating at supercritical speed.

Requirements of vision may dictate either a flat region near the nose of the windshield or single-curve surfaces. The pressure results of these tests indicate that it should be possible to provide a small flat region at or very near the nose of the windshield without deleterious effects, but if the flat region is too large or is placed back in the high-velocity region, the local loads may be greatly increased and separation with consequent high drag may result. Windshields with single-curve surfaces may be designed with no sacrifice in performance.

Another design consideration is ease of construction. The results of these tests indicate that simple, easily designed forms are quite as satisfactory both for low drag and for low loads as more complicated shapes. Flat plates, however, can find only limited use in a good windshield. They may possibly be used on the side or on the tail where the designed surface may be approximately flat already; and small flat plates may be used very close to the nose. Otherwise they are likely to cause increased local loads and high drags. The use of a design with single-curve surfaces should simplify the construction of the framework and its glass or metal covering. Retaining strips transverse to the air flow increase the drag (see reference 5) and may cause separation if placed near a negative pressure peak. They should therefore be avoided, and the surface of the windshield should be made smooth. If retaining strips must be used, they should, where possible, run in a direction parallel to the air flow and, in any case, they should be as thin as is consistent with strength requirements and as well faired as possible.

Satisfactory shapes may be designed by use of the shape characteristics of the five low-drag, low-load windshields, 2-0-3, 4-0-3, 3-1-2, X-1, X-2, presented in this report. (See fig. 1.) These characteristics, which already have been discussed, are: large fineness ratio, long noses and long tails, and, except at the nose and tail, well-rounded surfaces with no sharp corners or small radii of curvature. The 2-0-3, the 4-0-3, and the 3-1-2 windshields have double-curve surfaces and may therefore offer some difficulty in construction. The X-1 windshield has single-curve surfaces except for the top and should therefore be easy to build. The shape characteristics of the X-2 windshield will presently be discussed in detail.

A modification of the X-1 and X-2 windshields that is permissible and probably desirable is the rounding of the nose. A very small radius may also be given the tail without affecting the performance. Unless the stream flow is parallel to the axis of the windshield, the sharp nose on the X-1 and X-2 windshields may cause burbling with consequent drag increase, though for small angles of the flow the increase may be small. If the nose is rounded off to a small radius, it will be less sensitive to angularity of the flow.

If a windshield is desired having low peak negative pressures, that is, low peak loads and very high critical speed, particular attention must be paid to the shape. The 4-0-3 windshield is seen from figure 33 to meet this requirement reasonably well, although, as has already been pointed out, this windshield may be more difficult to construct than a windshield with single-curve surfaces. A new windshield, designated here the X-2 windshield, was designed to be constructed nearly similar to the X-1 windshield but with a negative pressure peak as low as that of the 4-0-3 and with drag as low as that of the X-1 windshield. These objectives were attempted in two ways: first by increasing the fineness ratio nearly to that of the 4-0-3 windshield, and second by modifying the form to give an approximately flat pressure distribution over the middle forward part of the windshield. An attempt was made to insure that the positive pressure gradient over the tail should be not greater than that over the tail of the X-1 windshield. The ordinates for this windshield and the manner of its construction have already been given. Unfortunately, the windshield was not constructed accurately according to these ordinates. The most important divergence was a fullness in the nose amounting to as much as 0.09 inch at the B-B plane (see fig. 3) just forward of the front negative pressure peak.

The main objectives sought have, nevertheless, been attained, as shown in figures 12, 24, and 33. Except for the unreliable upper and lower parts of the drag curve, explained previously, the drag is about the same as that of the X-1 windshield. Figure 24 shows that the pressure distribution is almost flat over the main forward part of the windshield; whereas a comparison with figure 23 shows that the pressure gradient is slightly less than that over the tail of the X-1 windshield. Figure 33 shows that the peak negative pressures on the new windshield were less than those on the 4-0-3 windshield and less than those of any of the other windshields tested. The peak negative pressure would probably have been somewhat lower if the windshield had been built accurately according to the ordinates given.

The X-2 windshield is considered to meet the requirement for a windshield having low local loads, high critical speed, and low drag. At the same time it should be reasonably easy to construct.

CONCLUSIONS

The pressure and drag results presented herein are strictly applicable only to the windshields in combination with the particular wing and fuselage used in these tests. They apply to windshields of the cockpit-canopy type as used on pursuit or similar types of airplane.

From the data obtained in the tests, the following conclusions were drawn:

1. The drag of a good windshield was found to be about 2 percent of the drag of a good airplane; the drag of a bad windshield might easily be 20 percent of the airplane drag.

2. The good windshields were characterized by long noses and tails and by the absence of sharp corners transverse to the flow.

L-462

3. The effect of compressibility within the range of Mach numbers of these tests was to increase greatly the drag of bad windshields.

4. Those windshields having high drags were also characterized by high local loads; some of those having low drags had moderately high local loads. The local loads varied greatly between different windshields.

5. Those windshields having low local loads were characterized by long noses and tail and by the absence of sharp corners transverse to the flow. In addition, the shapes of these windshields were such as to tend to distribute the load uniformly over the main body of the windshield.

6. The local loads on all windshields not having excessively high drags were found to increase markedly with increase in Mach number.

7. Interference from the wing and fuselage was found to have an important effect on the loads over a windshield. For the position of the windshield relative to the wing and fuselage as represented by these tests, the effect of interference was to increase the loads.

8. By the design of a new windshield, the X-2, reduction in both drag and local loads was found possible.

Langley Memorial Aeronautical Laboratory,
National Advisory Committee for Aeronautics,
Langley Field, Va.

APPENDIX

THE INFLUENCE OF WING AND FUSELAGE INTERFERENCE ON THE PRESSURES ACTING ON A WINDSHIELD

In any analysis of flow about windshields the effect of interference must be considered. Both loads and drags are dependent on the interference velocities due to the wing, the fuselage, and any other bodies near the windshield. Application of the results of these tests will depend on the interference experienced by the windshield on the airplane as compared with the interference due to the wing and fuselage on which the similar windshield was tested.

An estimate of the interference experienced in these tests and an example of the effect of this interference on the loads over one of the windshields tested will serve to show how the interference velocities for any combination may be approximately determined and, at the same time, will indicate the magnitude of the interference effects on the results presented in this report.

The general nature of the interference to be expected may be seen from figure 34, which shows the relative positions of the windshield, the wing, and the fuselage and their respective surface pressure distributions. As negative pressure coefficients correspond to positive velocity increments ΔV, it may be immediately deduced that the field of the wing and fuselage, extending outward, will produce at the position of the windshield, without the windshield in place, velocities v greater than the stream velocity. These induced velocities decrease with distance from the surface and follow a curve somewhat resembling an exponential damping curve. Thus, the closer the windshield is to the wing and fuselage, the greater is the effect of interference. The windshield is closer to the fuselage than to the wing, but the velocities over the wing are much greater and, as a result, the effect of the wing may be as great as or greater than that of the fuselage, particularly at high speeds, because of the extension of the field with Mach number.

In the quantitative discussion of interference, it is convenient to consider the velocity-increment coefficients $\Delta V/V$ and the resultant velocity coefficients v/V. The resultant velocity v is obtained by the vector addition of the velocity increment ΔV to the stream velocity V or to the velocity otherwise existing at the point, but for small values of ΔV and for usual positions of the windshield, a sufficiently good approximation may be obtained by adding these quantities arithmetically. The velocity increment v/V may be obtained according to Bernoulli's equation from the pressure coefficient P by the relation

$$\frac{v}{V} = \sqrt{1 - \frac{2}{(\gamma - 1)M^2}\left[\left(1 + \frac{\gamma}{2} PM^2\right)^{\frac{\gamma-1}{\gamma}} - 1\right]}$$

or at low speeds by the incompressible-flow relation

$$\frac{v}{V} = \sqrt{1 - P_i}$$

Before the effect of interference due to the wing and fuselage can be quantitatively estimated, the velocity increments due to these bodies must be determined. Velocity contours, that is, lines of equal value of v/V for a portion of the field of the NACA 2215 airfoil at $\alpha = -0.67^\circ$, have been determined by the method of reference 8 and are given in figure 35. It may be remarked that the velocity field as much as one chord length from the surface will be nearly the same for other wings of the same thickness ratio and at the same lift coefficient as for this one. Thus, the interference on a body located as much as a chord length away from a wing could be obtained to a sufficiently good approximation from the field of a Joukowski airfoil of the same thickness ratio and with the same lift coefficient, the Joukowski airfoil having the advantage of being mathematically tractable. Closer to the wing the velocities are more and more influenced by the particular profile form.

As seen in figure 35, the velocity coefficient falls off rapidly with distance from the surface. If a line through the point on the surface corresponding to peak velocity is drawn parallel to the chord line, the decay of peak velocity with distance perpendicular to this line is as shown in figure 36 for $M = 0$. About the same decay curve was found theoretically for the 11.9-percent-thick symmetrical Joukowski airfoil at 0° and 4° angle of attack and experimentally for the 18.8-percent-thick airfoil at

$C_L = 1.6$ given in reference 9. The decay curve is probably not much different for any other airfoil of approximately similar shape.

The compressibility effect on the field shown in figure 35 may be obtained by increasing the distances from the wing chord for all points on the velocity contours in the ratio $1/\sqrt{1 - M^2}$ (references 10 and 11). The corresponding values of the velocity-increment coefficient $\left(\frac{\Delta V}{V} = \frac{v}{V} - 1\right)$ may then be increased in the same ratio to obtain the contour plot for any given Mach number (reference 10). The compressibility effect was applied in figure 36 for $M = 0.40$, 0.60, 0.70, and 0.80 by shifting all points on the curve for $M = 0$ to the right in the ratio of abscissas $1/\sqrt{1 - M^2}$.

The pressures measured on the fuselage are subject to interference from the wing and consequently cannot be directly used for the estimation of fuselage interference. Approximate interference velocities may be obtained by replacing the body by its equivalent prolate spheroid, as shown in figure 37. The peak velocity-increment coefficients $\Delta V/V$ are 0.21, 0.12, 0.08, and 0.03 for prolate spheroids of fineness ratios 2, 3, 4, and 8, respectively. Figure 37 gives the corresponding decay curves. The extension of the field with Mach number is given only for the fineness ratio 4. In the absence of any rigorous theory concerning the effect of compressibility on the velocity field about a body of revolution, the same compressibility effect will be assumed for the fuselage as is used for the wing.

The velocity-increment coefficients at the surface of the fuselage without the wing interference were actually obtained, however, by deducting the velocity coefficients in the field of the wing (fig. 35) at the positions of the fuselage orifices from the corresponding velocity coefficients determined from the pressures measured at these orifices. The velocity coefficients from the measured pressures and the estimated wing interference from figure 35 for the top and side orifice lines on the fuselage are shown in figure 38. The difference, shown as the velocity-increment coefficient $\Delta V/V$, is less for the top than for the side meridian. This result may be partly due to overcorrection, but the velocity over the top should be somewhat smaller because the fuselage is more nearly flat at the top. Also, the dip in the curves is expected because of the near flatness of the fuselage in this region. The decay curves of figure

37 may be applied to the $\Delta V/V$ values of figure 38 for estimating the interference velocities off the surface. The particular decay curve corresponding to the fineness ratio of the prolate spheroid that can be most nearly fitted to the fuselage should be used.

As an example, the interference effects with the X-1 windshield have been estimated. Since the velocities are highest at orifice line 4, the velocity coefficients at this line will be reduced to the approximate values characteristic of the windshield alone, that is, no interference. The location of the windshield with orifice line 4 is given in figure 35, from which the corresponding interference velocities from the wing at low speed can be obtained. For the fuselage interference, the diameter of the fuselage is 12 inches and the length of the equivalent prolate spheroid about 75 inches, and the fineness ratio therefore about 6. Windshield orifice line 4 is about 2 inches or about 0.17 the fuselage diameter from the surface of the fuselage. Thus, by interpolation for a fineness ratio of 6 in figure 37, the $\Delta V/\Delta V_{max}$ ratio at 0.17 the diameter from the surface is about 0.80. By multiplying the velocity ratio $\Delta V/V$ at the top meridian (fig. 38) by 0.80, the velocity-increment coefficients due to the fuselage interference at windshield orifice line 4 may be determined. The interference velocities $\left(\frac{v}{V} = 1 + \frac{\Delta V}{V}\right)$ are shown with the velocity distribution on the windshield in figure 39. The total interference velocity, shown in the same figure, is obtained by adding to unity the increments due to the wing and to the fuselage,

$$\text{Total interference-velocity coefficient} = 1 + \left(\frac{\Delta V}{V}\right)_{wing} + \left(\frac{\Delta V}{V}\right)_{fuselage}$$

Curve A, which shows the windshield velocity distribution with the interference removed, was obtained by dividing the windshield velocity ratios given in the top curve by the corresponding velocity ratios v/V taken from the curve showing total interference.

Figure 40 shows somewhat the same effects, complicated, however, by compressibility. The wing interference was obtained by increasing the distances perpendicular to the wing of all points on the velocity contours of figure 35 in the ratio $1/\sqrt{1 - M^2}$ and increasing all $\Delta V/V$ values by the factor $1/\sqrt{1 - M^2}$, thus changing both the position and the values of the velocity contours. The fuselage interference was obtained by increasing the $\Delta V/V$ values of figure 38 in the ratio $1/\sqrt{1 - M^2}$ and interpolating among the decay curves of figure 37 for a fineness ratio of 6 and Mach number 0.688 at 0.17 the diameter from the surface. The total interference was obtained as before by adding the wing and fuselage induced velocity coefficients. The windshield velocity coefficients could then have been corrected as in figure 39, but actually the reverse process was applied. Because of the interference the windshield is subject to a Mach number approximately equal to the product of the interference velocity v/V with the stream Mach number, which in this case is 0.688. The interference Mach numbers are given on the total-interference curve of figure 40. Curve A, from figure 39, was then raised by multiplication of the velocity-increment coefficients $\left(\frac{\Delta V}{V} = \frac{v}{V} - 1\right)$ with $1/\sqrt{1 - M^2}$, using the local Mach numbers shown. The resulting curve was raised again by multiplication with the interference velocities v/V to give a curve of the final estimated velocity on the windshield. The proximity of this curve to the curve of velocities obtained from the pressure measurements is an indication of the validity of the assumptions concerning the effect of compressibility on interference. Figure 40 shows that the interference effect may become very great at high speeds. At still higher speeds, above the critical speed of the wing, the effect is still greater; but since at speeds above the critical the Mach number effect, either on the interference or on the velocities without interference, is quantitatively unknown, it cannot be estimated with any degree of accuracy.

As a check on the approximate correctness of the estimated interference effect, the velocity coefficients for the 4-0-3 windshield were adjusted as for the X-1 windshields. This windshield is approximately one-half the 111 body of revolution cut along the longitudinal axis (reference 12), and the calculated velocity distribution for this body is given along with that of the measured and adjusted distributions for the 4-0-3 windshield in figure 41. Although the shape of the windshield velocity-distribution curve departs considerably from the theoretical shape for the 111 body, the fact that the adjusted curve falls near the theoretical indicates that the estimated interference was approximately equal to the interference actually experienced.

The effect of interference on loads has not been specifically given in this example since it was convenient to discuss velocities rather than pressures; but the pressure coefficients may easily be obtained from the velocity coefficients either at low speeds by the incompressible flow relation

$$P_i = 1 - \left(\frac{v}{V}\right)^2$$

or at high speeds by

$$P = \frac{2}{\gamma M^2}\left\{1 - \frac{\gamma - 1}{2} M^2 \left[\left(\frac{v}{V}\right)^2 - 1\right]\right\}^{\frac{\gamma}{\gamma - 1}} - \frac{2}{\gamma M^2}$$

where for air γ is approximately 1.4. The pressure coefficients P are roughly double the velocity-increment coefficients $\left(\frac{\Delta V}{V} = \frac{v}{V} - 1\right)$.

The windshield drag results are not considered sufficiently accurate to justify the quantitative estimation of interference effects, but an approximate value of the windshield drag coefficient referred to the increased velocity field due to the interference velocities may be obtained by dividing the windshield drag coefficient $C_{D_{F_W}}$ by the square of the interference velocity coefficient v/V. Thus, if the interference velocity coefficient is 1.05 (as shown in fig. 39), the windshield drag coefficient is reduced by about 10 percent. That is, the drag coefficient given is about 10 percent greater than would have been obtained if the interference velocities had been zero.

The interference effect of the X-1 windshield on the model will now be considered. The drag and negative pressure coefficients on the wing and fuselage, except for the part of the fuselage covered by the windshield, are generally slightly increased by interference velocities due to the windshield, but the most important effect is the lowering of the critical speed of the wing. The interference velocities in the field of the windshield can be found in the same way as for the fuselage. If the thickness of the X-1 windshield is taken to be 6 inches and the fineness ratio of the equivalent prolate spheroid to be 3, a peak surface velocity coefficient of 1.26 being assumed (fig. 40), the velocity off the surface may be estimated from figure 37. The distance from the surface of the wing to windshield orifice line 4 is is about 12.4 inches or slightly over two windshield diameters. From figure 37 the corresponding $\Delta V/\Delta V_{max}$ value for $M = 0.688$ was found to be 0.085. The velocity-increment coefficient 0.26 was multiplied by this value to obtain 0.022 for the increment due to interference of the windshield on the wing. Thus, the effective velocity at the wing might be as much as 2 percent greater than the stream velocity. The effective Mach number is increased by approximately the same percentage, from 0.688 to 0.702, or otherwise the apparent critical speed of the wing is lowered by this amount. The windshield interference will, of course, affect the wing over only a limited region; but the resulting drag increase when the critical speed of the wing is reached locally in this region will be of the same order of magnitude as the increase that would have been experienced had the critical speed of the windshield itself been attained.

The methods herein presented for estimating the effect of interference are based on smooth flow. If separation occurs, the effect of interference cannot be determined.

REFERENCES

1. Hartley, J. H., Cameron, D., and Curtis, W. H.: Note on Wind Tunnel Tests on the Design of Cabins. R. & M. No. 1811, British A.R.C., 1937.

2. Jacobs, Eastman N.: The Reduction in Drag of a Forward-Sloping Windshield. N CA TN No. 481, 1933.

3. Clay, William C.: Improved Airplane Windshields to Provide Vision in Stormy Weather. NACA Rep. No. 498, 1934.

4. Serby, J. E.: Pilots' View in Cabin Aircraft. Aircraft Engineering, vol. X, no. 113, July 1938, pp. 219-20.

5. Robinson, Russell G., and Delano, James B.: An Investigation of the Drag of Windshields in the 8-Foot High-Speed Wind Tunnel. NACA Rep. No. 730, 1942.

6. Robinson, Russell G.: Sphere Tests in the N.A.C.A. 8-Foot High-Speed Tunnel. Jour. Aero. Sci., vol. 4, no. 5, March 1937, pp. 199-201.

7. Hood, Manley J.: The Effects of Some Common Surface Irregularities on Wing Drag. NACA TN No. 695, 1939.

8. Jones, Robert T., and Cohen, Doris: A Graphical Method of Determining Pressure Distribution in Two-Dimensional Flow. NACA Rep. No. 722, 1941.

9. Bryant, L. W., and Williams, D. H.: An Investigation of the Flow of Air around an Aerofoil of Infinite Span. R. & M. No. 989, British A.R.C., 1924.

10. Ackeret, J.: Über Luftkräfte bei sehr grossen Geschwindigkeiten insbesondere bei ebenen Strömungen. Helvetica Physica Acta, vol. I, fasc. 5, June 4, 1928, pp. 301-22.

11. Prandtl, L.: General Considerations on the Flow of Compressible Fluids. NACA TM No. 805, 1936.

12. Abbott, Ira H.: Fuselage-Drag Tests in the Variable-Density Wind Tunnel: Streamline Bodies of Revolution, Fineness Ratio of 5. NACA TN No. 614, 1937.

TABLE I
ORDINATES FOR WINDSHIELD NOSE AND TAIL PIECES

[All dimensions are in inches, r is the radius of the circumscribed circle]

N-2

x	r
0.23	0.73
.45	1.10
.90	1.65
1.80	2.35
3.61	3.11
5.41	3.43
7.00	3.50

N-3

x	r
0.34	0.73
.68	1.10
1.35	1.65
2.71	2.35
5.41	3.11
8.12	3.43
10.50	3.50

N-4

x	r
0.44	0.73
.88	1.10
1.75	1.65
3.50	2.35
7.00	3.11
10.50	3.43
13.59	3.50

T-1

x	r
0	3.50
1.28	3.40
2.42	3.11
3.57	2.57
4.71	1.80
5.27	1.38
5.86	.93
6.41	.47
7.00	0

T-2

x	r
0	3.50
2.56	3.40
4.85	3.11
7.13	2.57
9.42	1.80
10.53	1.38
11.71	.93
12.82	.47
14.00	0

T-3

x	r
0	3.50
3.91	3.40
7.41	3.11
10.91	2.57
14.41	1.80
16.11	1.38
17.91	.93
19.61	.47
21.41	0

T-4

x	r
0	3.66
3.91	3.55
7.41	3.25
10.91	2.69
14.41	1.88
16.11	1.44
17.91	.97
19.61	.49
21.41	0

T-5

x	r
0	3.78
3.91	3.67
7.41	3.35
10.91	2.78
14.41	1.95
16.11	1.49
17.91	1.00
19.61	.51
21.41	0

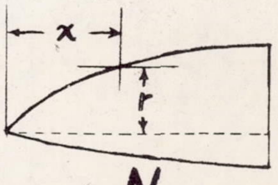

N

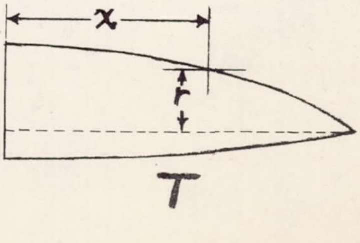

T

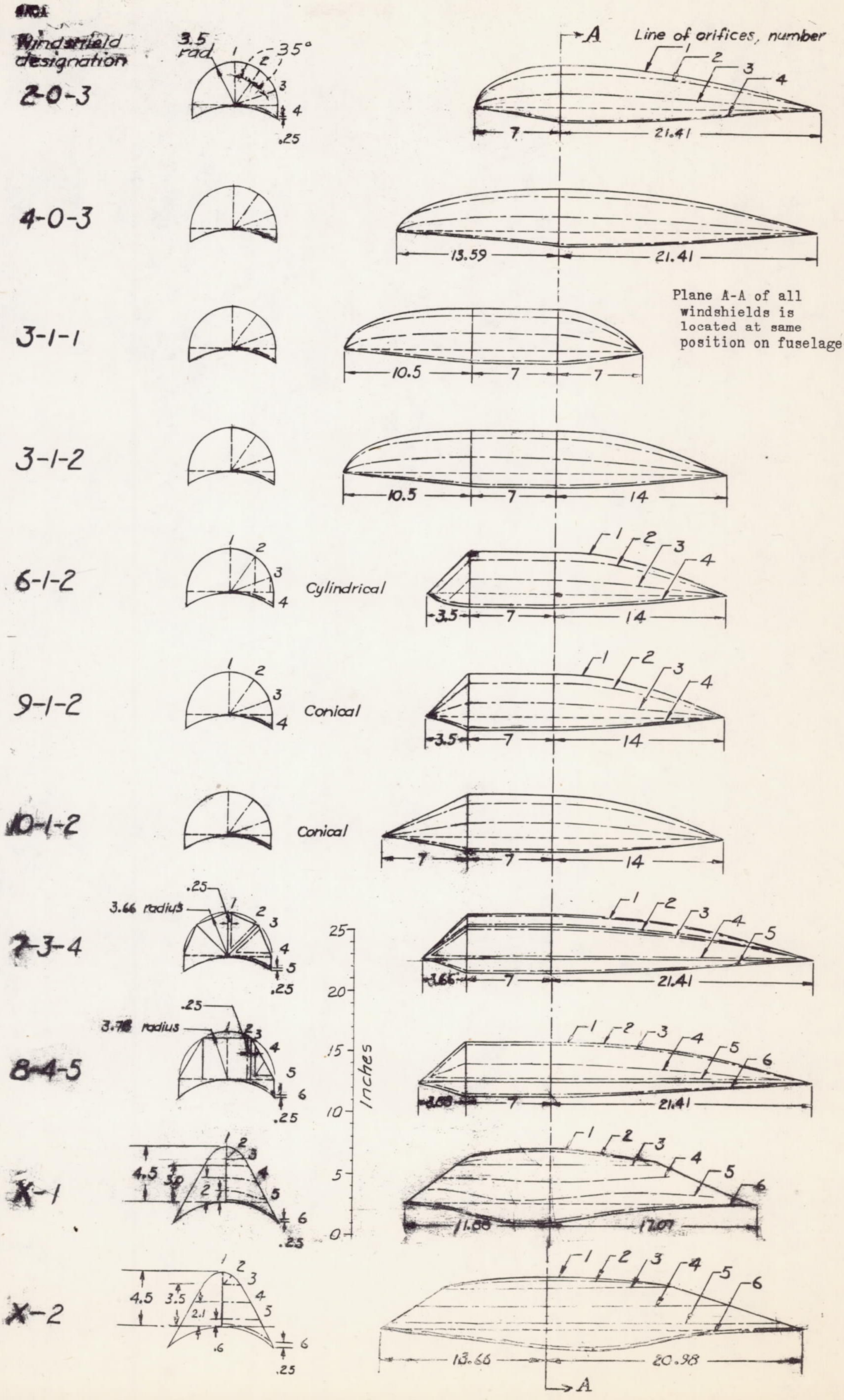
Windshield designation
2-0-3
3.5 rad
35°
1
2
3
4
.25
A
Line of orifices, number
1
2
3
4
7
21.41
4-0-3
13.59
21.41
3-1-1
10.5
7
7
3-1-2
10.5
7
14
6-1-2
Cylindrical
1
2
3
4
3.5
7
14
9-1-2
Conical
1
2
3
4
3.5
7
14
10-1-2
Conical
7
7
14
7-3-4
.25
3.66 radius
1
2
3
4
5
.25
3.66
7
21.41
8-4-5
.25
3.78 radius
1
2
3
4
5
6
.25
3.88
7
21.41
25
20
15
10
5
0
Inches
X-1
4.5
3.0
2
1
2
3
4
5
6
.25
11.88
17.07
X-2
4.5
3.5
2.1
.6
1
2
3
4
5
6
.25
13.66
20.98
A

Plane A-A of all windshields is located at same position on fuselage.

Figure 1.- Windshields and orifice locations. All dimensions are in inches.

X – 1 Ordinates

x_1	y_1	h
1	0.52	0.42
2	.90	.64
3	1.20	.78
4	1.42	.89
5	1.53	.96
6	1.56	.98
7	1.55	1.00
8	1.47	.97
9	1.37	.93
10	1.24	.86
11	1.08	.75
12	.90	.66
14	.47	.35
15.88	0	0

x_2	y_2
1	0.67
2	1.25
3	1.75
4	2.25
5	2.50
6	2.72
7	2.88
8	3.00
9	3.08
10	3.09
11	3.05
12	2.98
13	2.88
14	2.75
15	2.63
16	2.46
17	2.27
18	2.08
20	1.70
22	1.10
24	.56
26.12	0

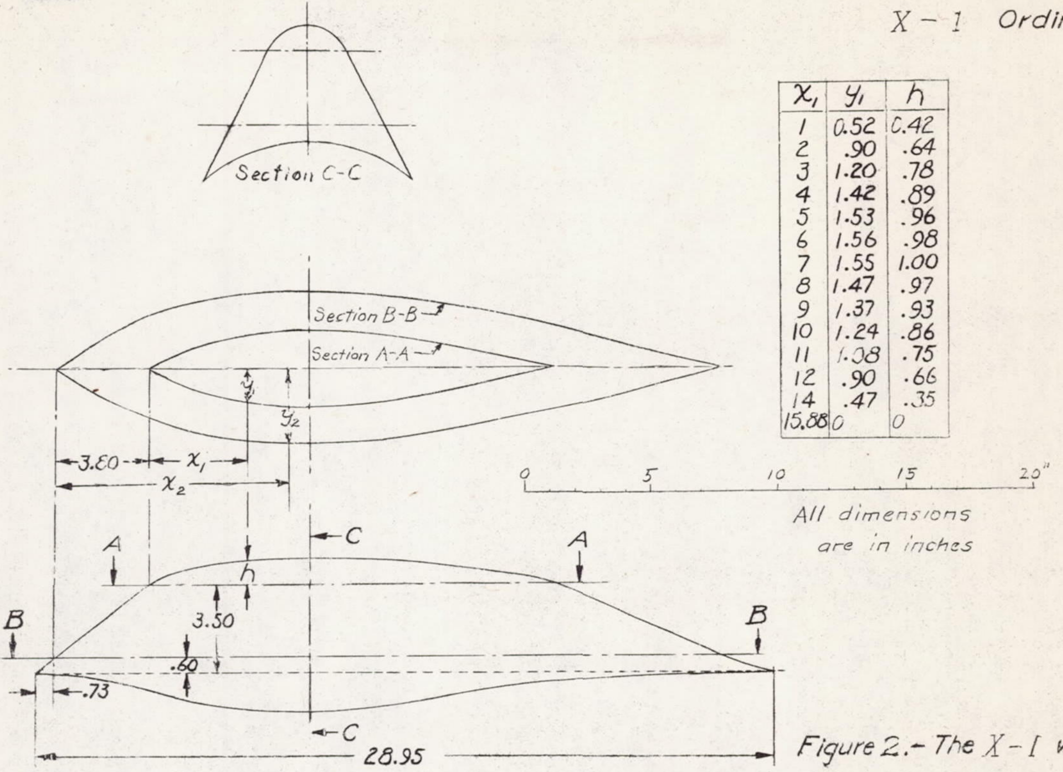
Section C-C
Section B-B
Section A-A
y_1
y_2
3.80
x_1
x_2
C
A
A
h
3.50
B
B
.60
.73
C
28.95
0
5
10
15
20"
All dimensions
are in inches

Figure 2.- The X-1 windshield.

X-2 Ordinates

x_1	y_1	h
0	0	0
.29	.202	.15
.57	.419	.30
1.06	.591	.38
1.44	.730	.48
1.82	.845	.54
2.21	.942	.61
3.17	1.125	.74
4.13	1.275	.83
5.09	1.387	.90
6.05	1.473	.95
7.01	1.521	.99
7.97	1.544	1.00
8.55	1.561	1.00
9.89	1.540	.98
10.85	1.476	.94
11.81	1.377	.89
12.78	1.262	.83
13.74	1.108	.75
14.69	.935	.65
15.65	.743	.55
16.51	.542	.43
17.58	.344	.29
18.54	.150	.13
19.37	0	0

x_2	y_2
0	0
.48	.387
1.11	.828
1.75	1.174
2.38	1.450
3.02	1.684
3.65	1.865
5.28	2.230
6.82	2.524
8.40	2.738
9.99	2.918
11.58	3.016
13.16	3.078
14.12	3.091
16.33	3.050
17.92	2.923
19.50	2.730
21.08	2.500
22.68	2.193
24.26	1.851
25.85	1.475
27.43	1.075
29.01	.682
30.58	.295
32.01	0

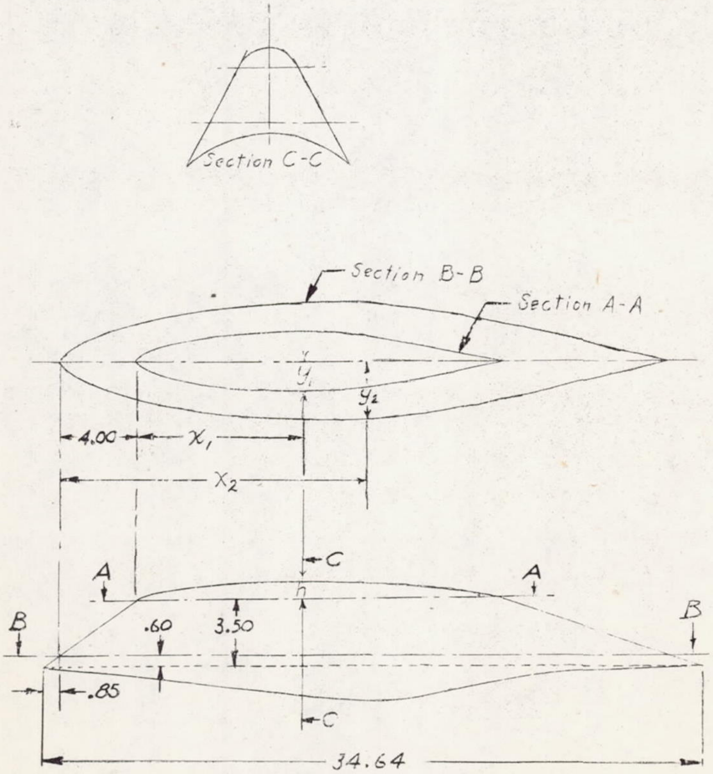
Section C-C
Section B-B
Section A-A
y_1
y_2
4.00
x_1
x_2
C
A
A
h
B
B
.60
3.50
.85
C
34.64

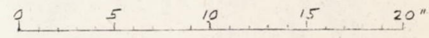

All dimensions are in inches

Figure 3.- The X-2 windshield.

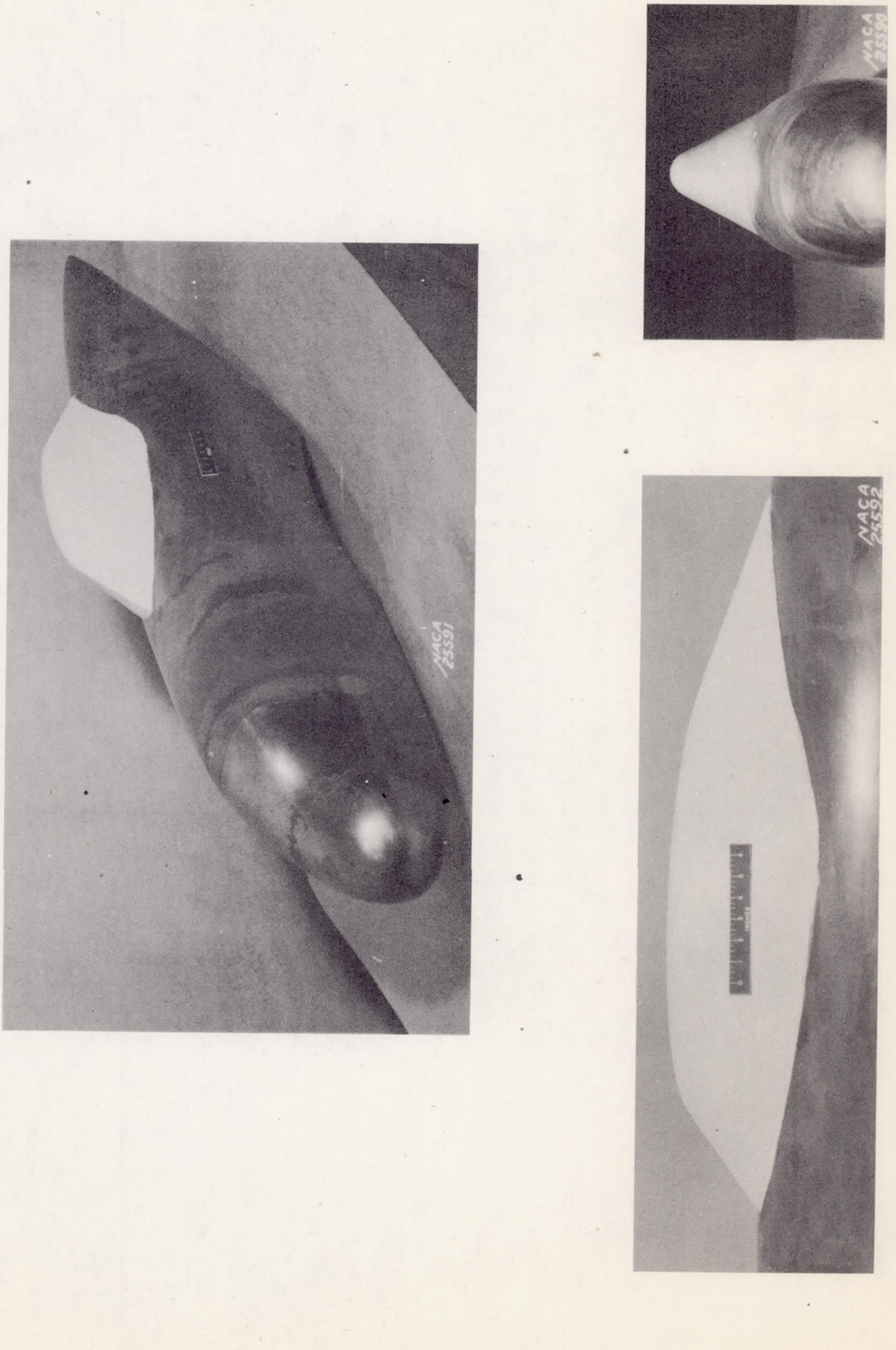
NACA 25591
NACA 25590
NACA 25592

Figure 4.- The X-2 windshield installation.

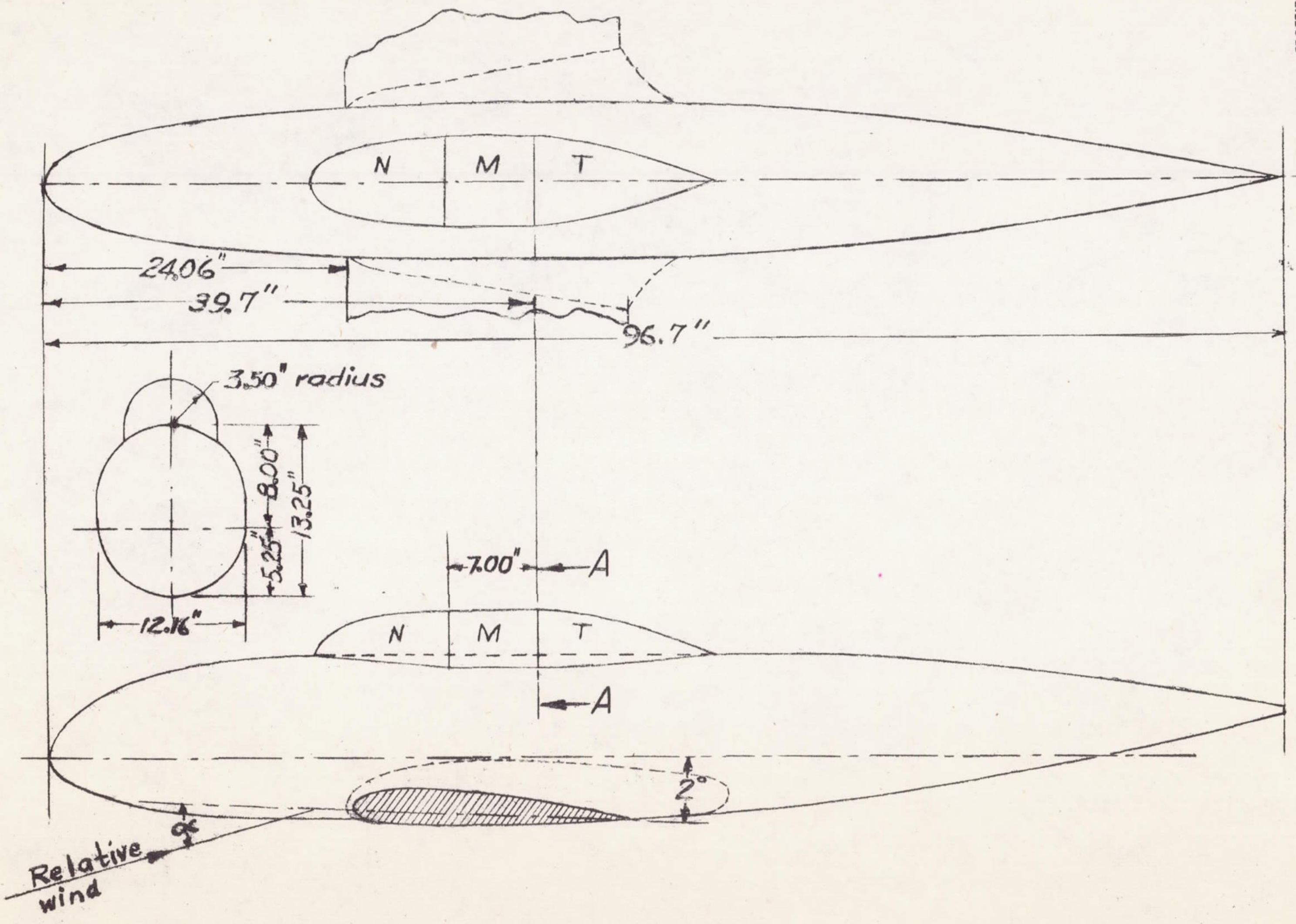
N
M
T
24.06"
39.7"
96.7"
3.50" radius
8.00"
13.25"
5.25"
12.16"
7.00"
A
A
2°
α
Relative wind

Figure 5.- Typical windshield installation.

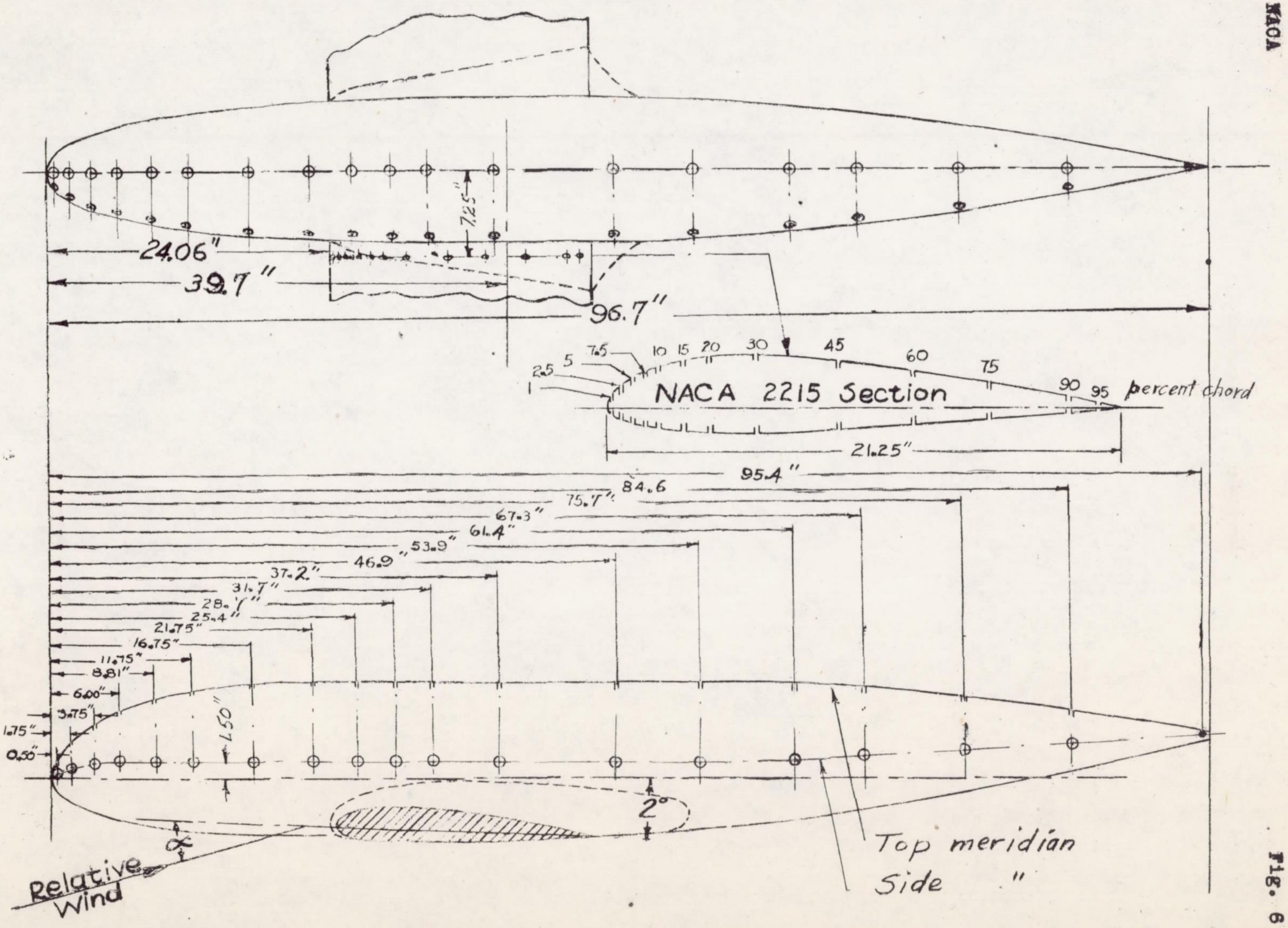
7.25"
24.06"
39.7"
96.7"
1
2.5
5
7.5
10
15
20
30
45
60
75
90
95
percent chord
NACA 2215 Section
21.25"
95.4"
84.6
75.7"
67.3"
61.4"
53.9"
46.9"
37.2"
31.7"
28.7"
25.4"
21.75"
16.75"
11.75"
8.81"
6.00"
3.75"
1.75"
0.50"
4.50"
2°
α
Top meridian
Side "
Relative Wind

Figure 6. - Pressure-orifice locations on wing and fuselage

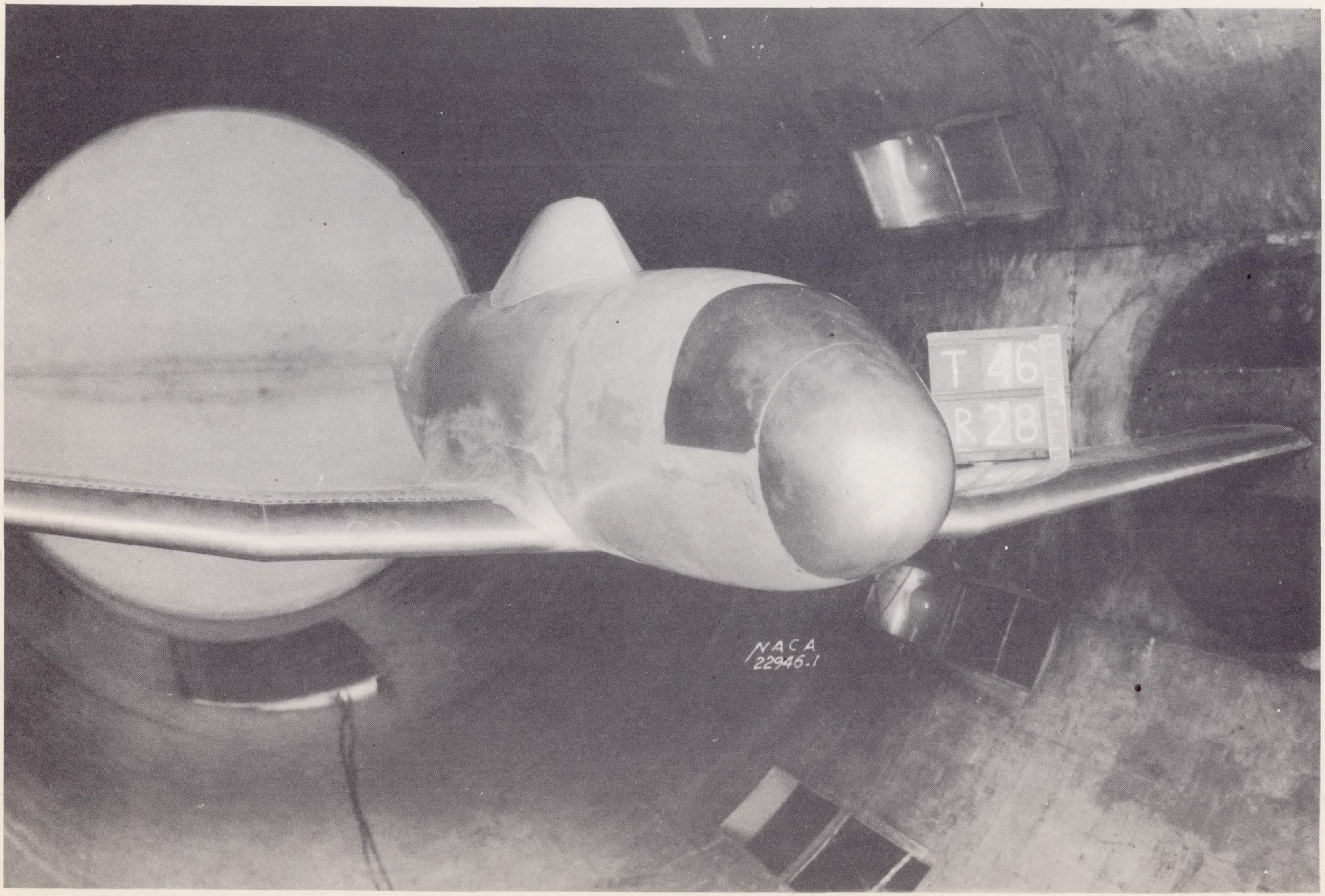
T 46
R28
NACA
22946.1

Figure 7.- Model installation in the tunnel showing the X-1 windshield.

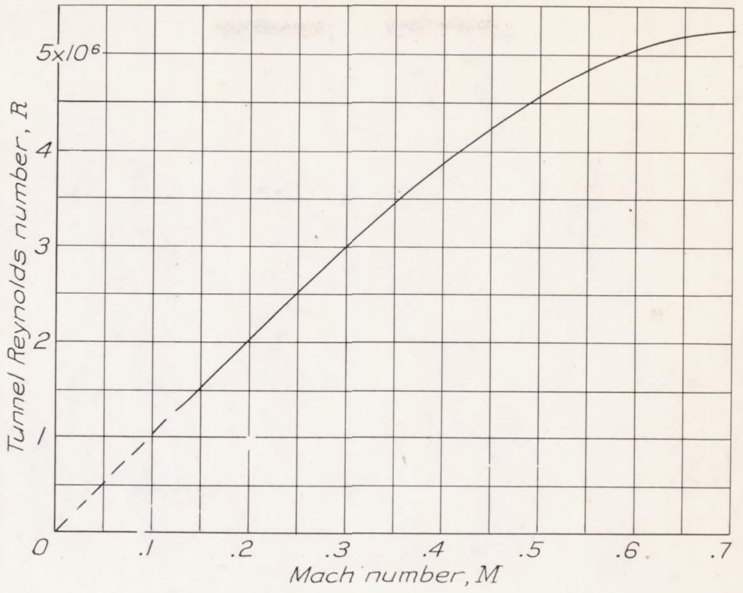

Figure 8.- Variation of test Reynolds number with Mach number.

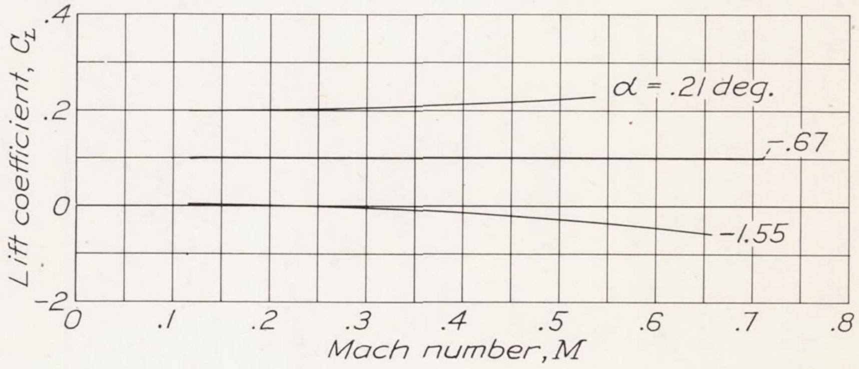

Figure 10.- Variation of model lift coefficient with Mach number.

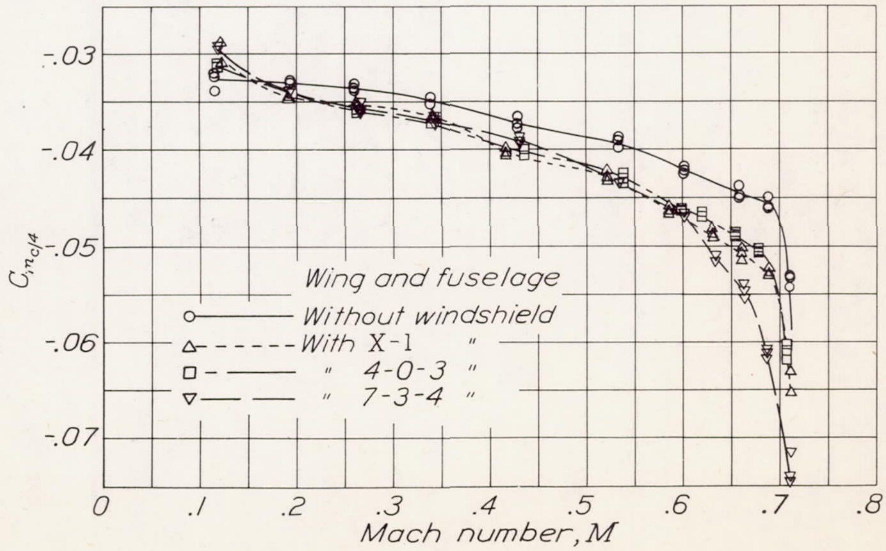

Figure 13.- Variation of model pitching-moment coefficient with Mach number. α, -0.67°.

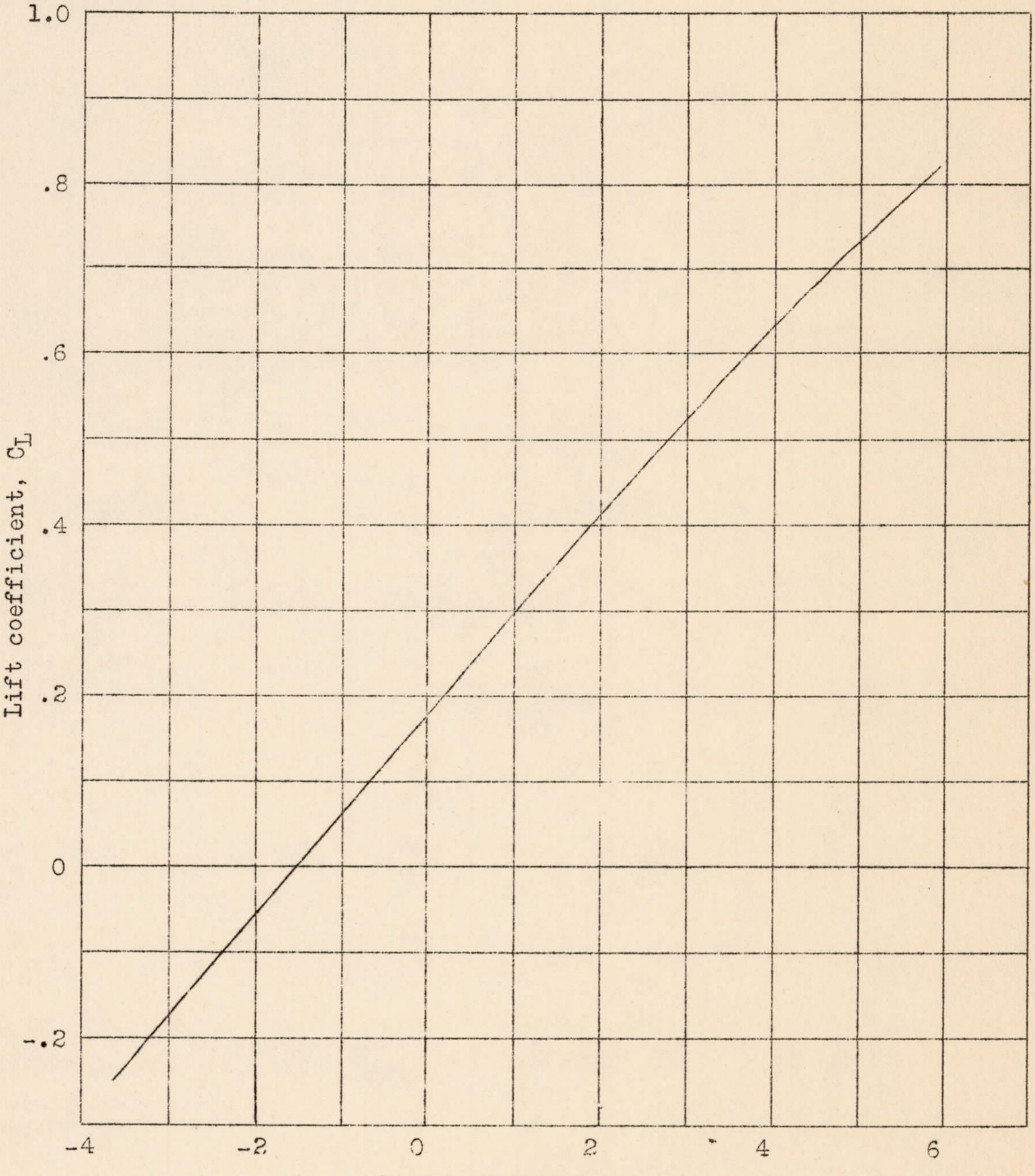

Figure 9.- Variation of model lift coefficient with angle of attack.
M, 0.193; R, 1,980,000.

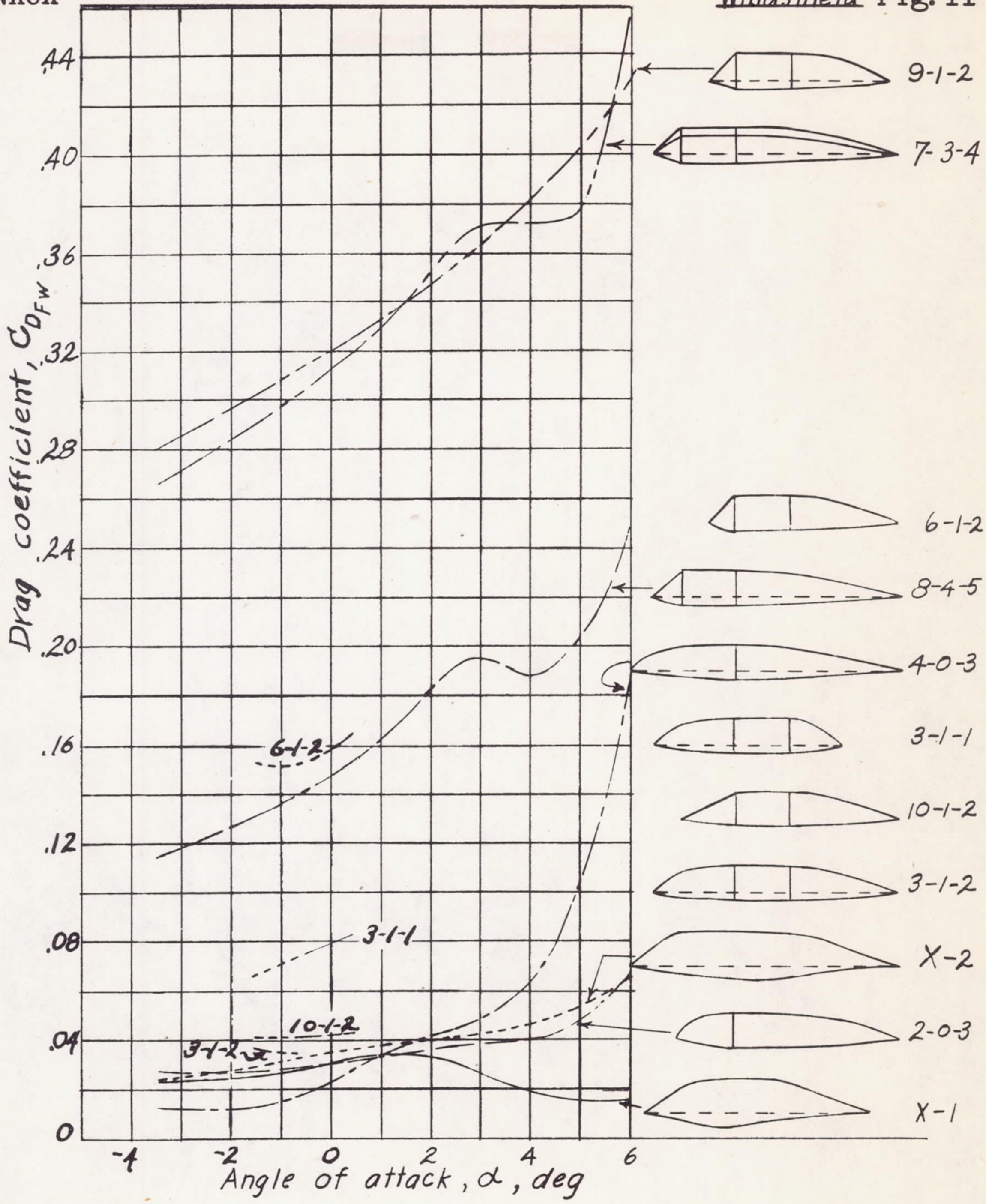

Figure 11.- Variation of windshield drag coefficient with angle of attack. M,0.193; R, 1,980,000.

NATIONAL ADVISORY
COMMITTEE FOR AERONAUTICS

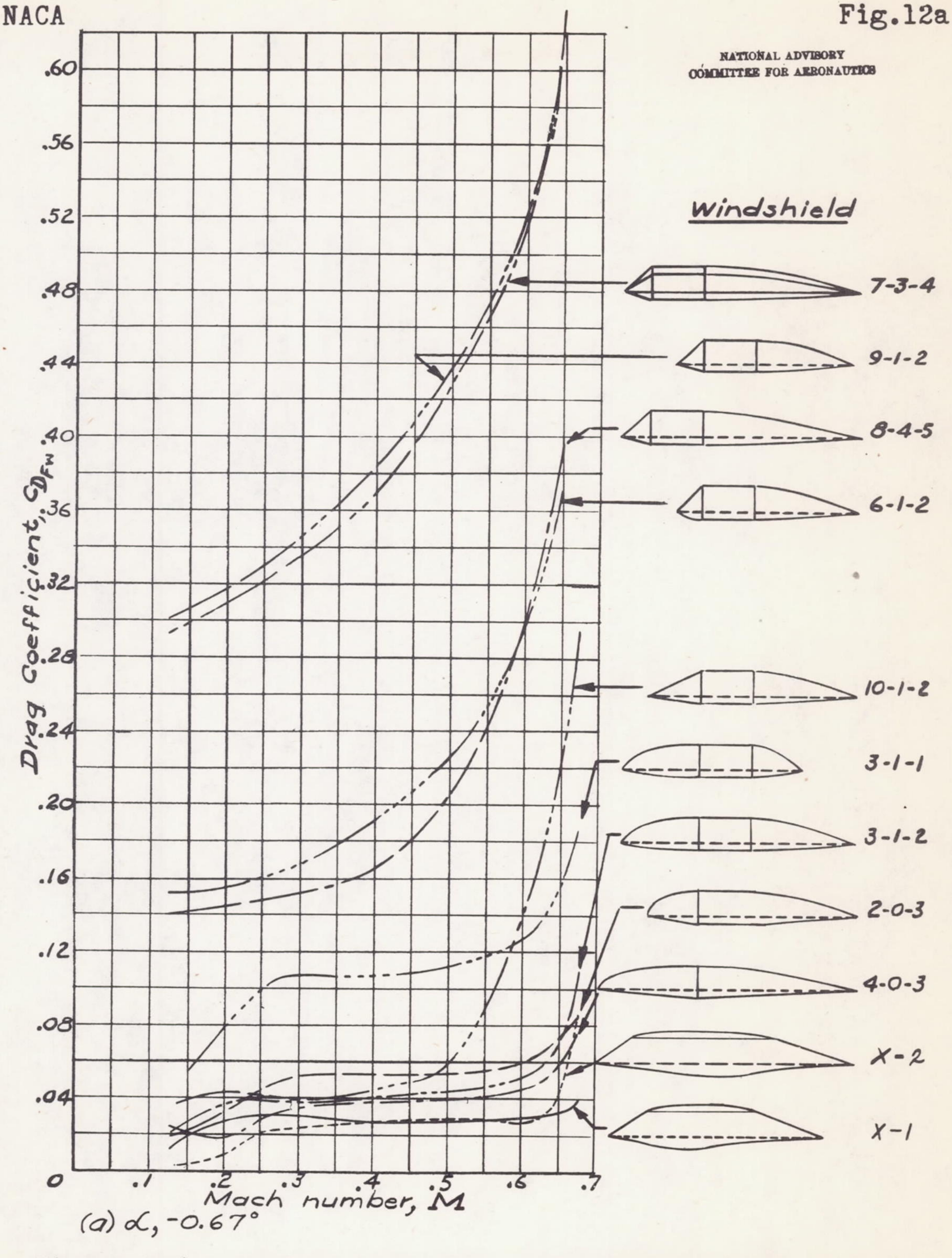

(a) α, -0.67°

Figure 12(a,b).- Variation of windshield drag coefficient with Mach number.

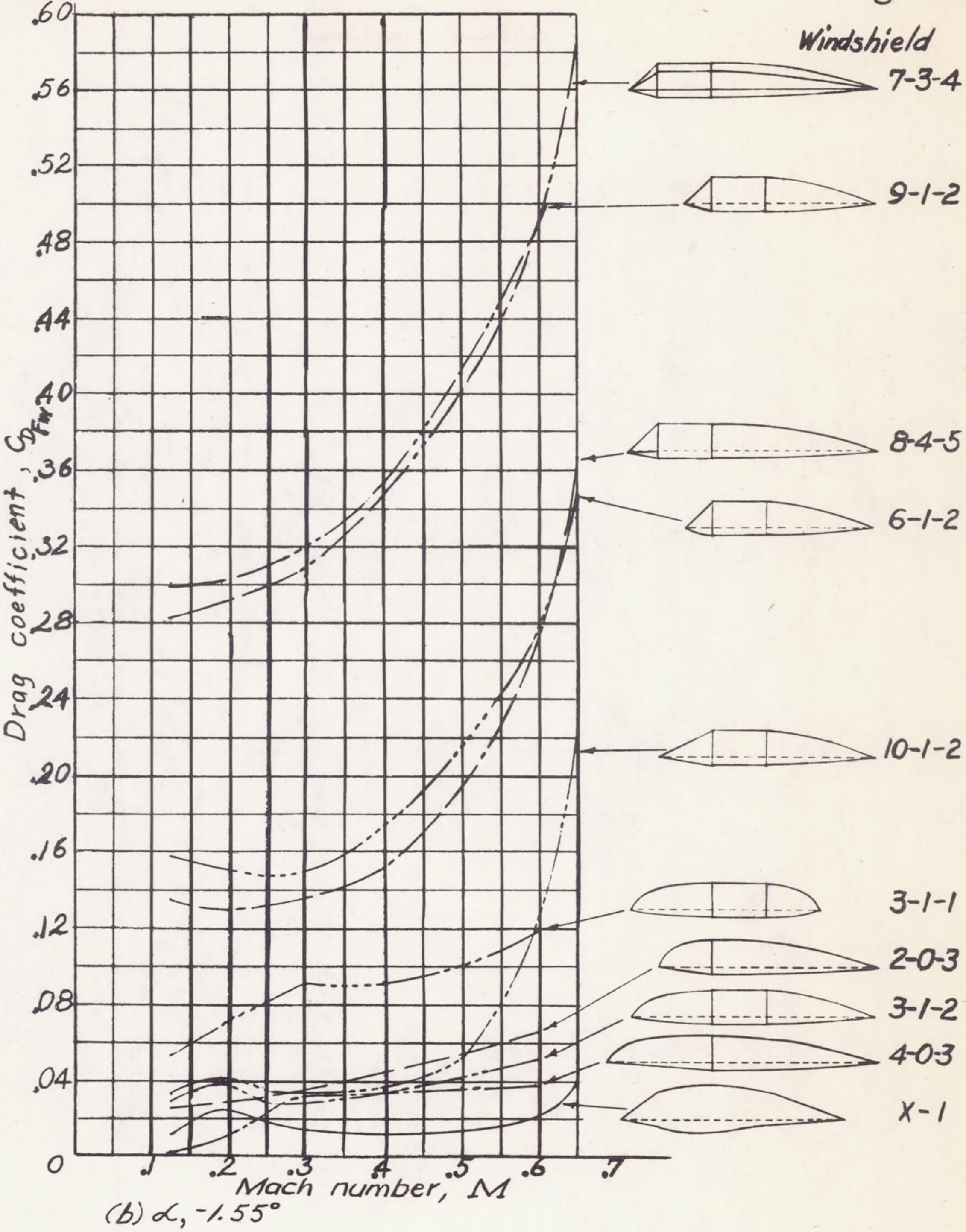

(b) α, -1.55°

Figure 12b.

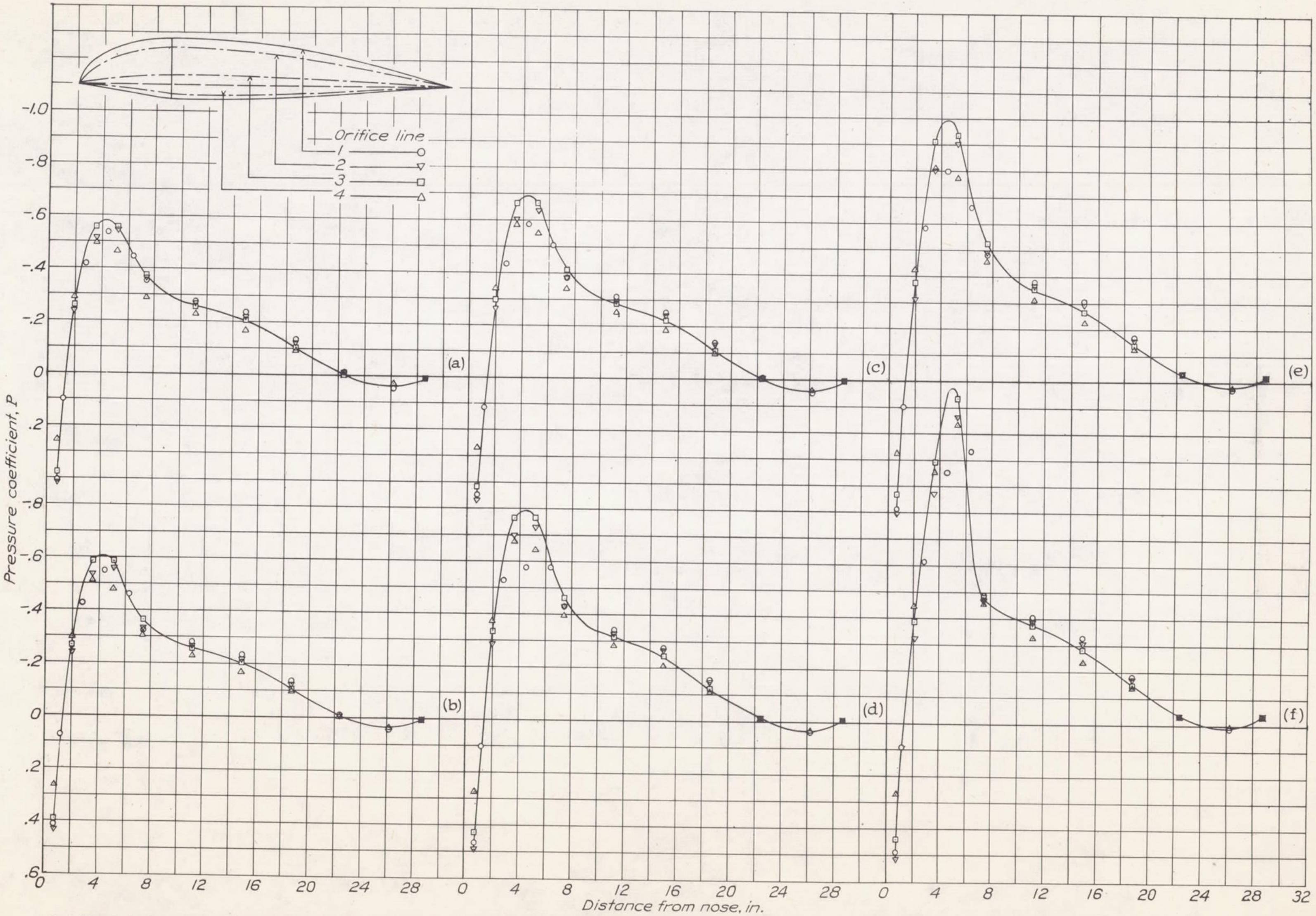

(a) M, 0.199 (b) M, 0.340 (c) M, 0.535 (d) M, 0.632 (e) M, 0.689 (f) M, 0.716

Figure 14.- Pressure distribution about the 2-0-3 windshield for various Mach numbers. α , -0.67°.

L - 462

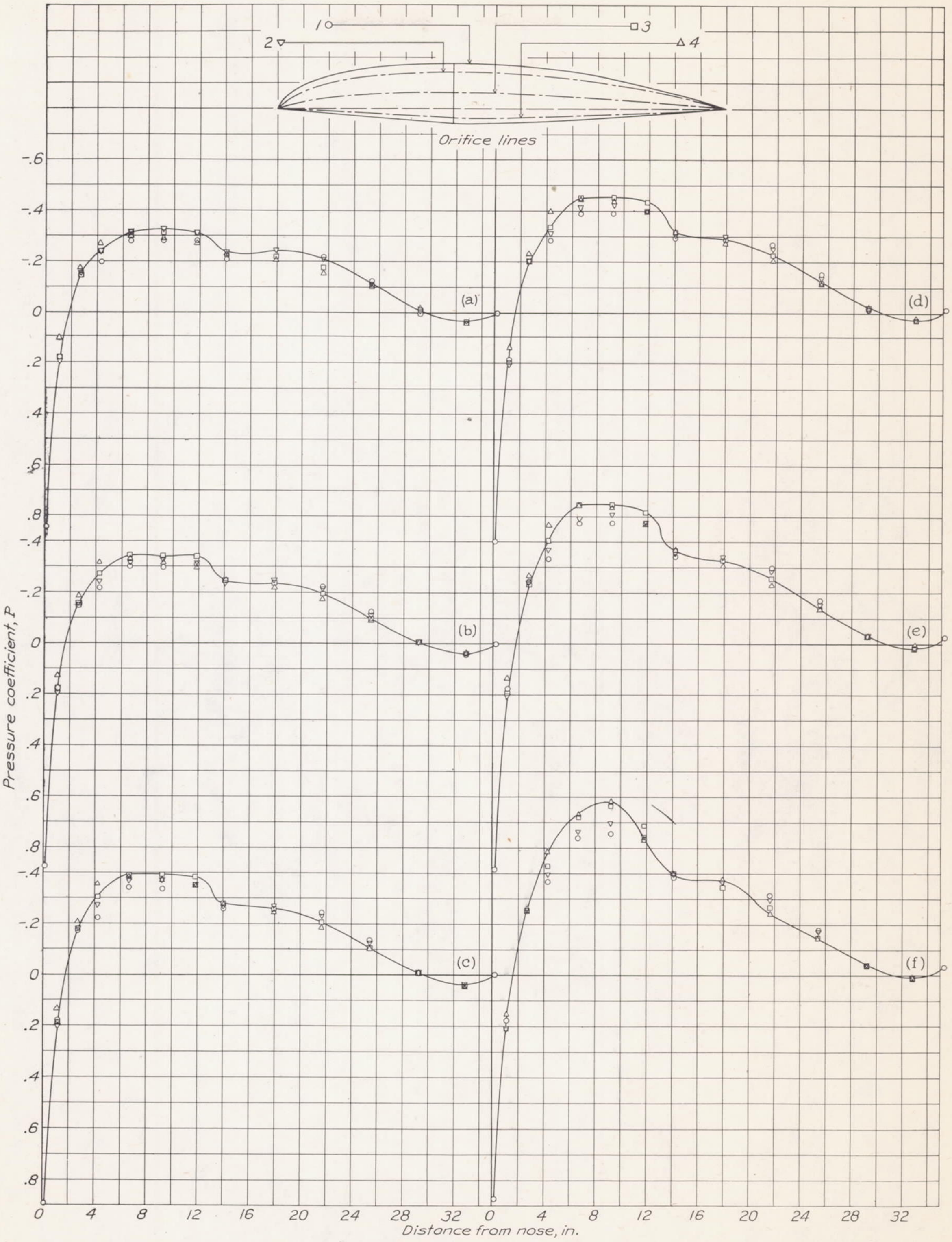

(a) M , 0.197 (b) M , 0.340 (c) M , 0.539 (d) M , 0.620 (e) M , 0.677 (f) M , 0.707

Figure 15.- Pressure distribution about the 4-0-3 windshield for various Mach numbers. α , -0.67°.

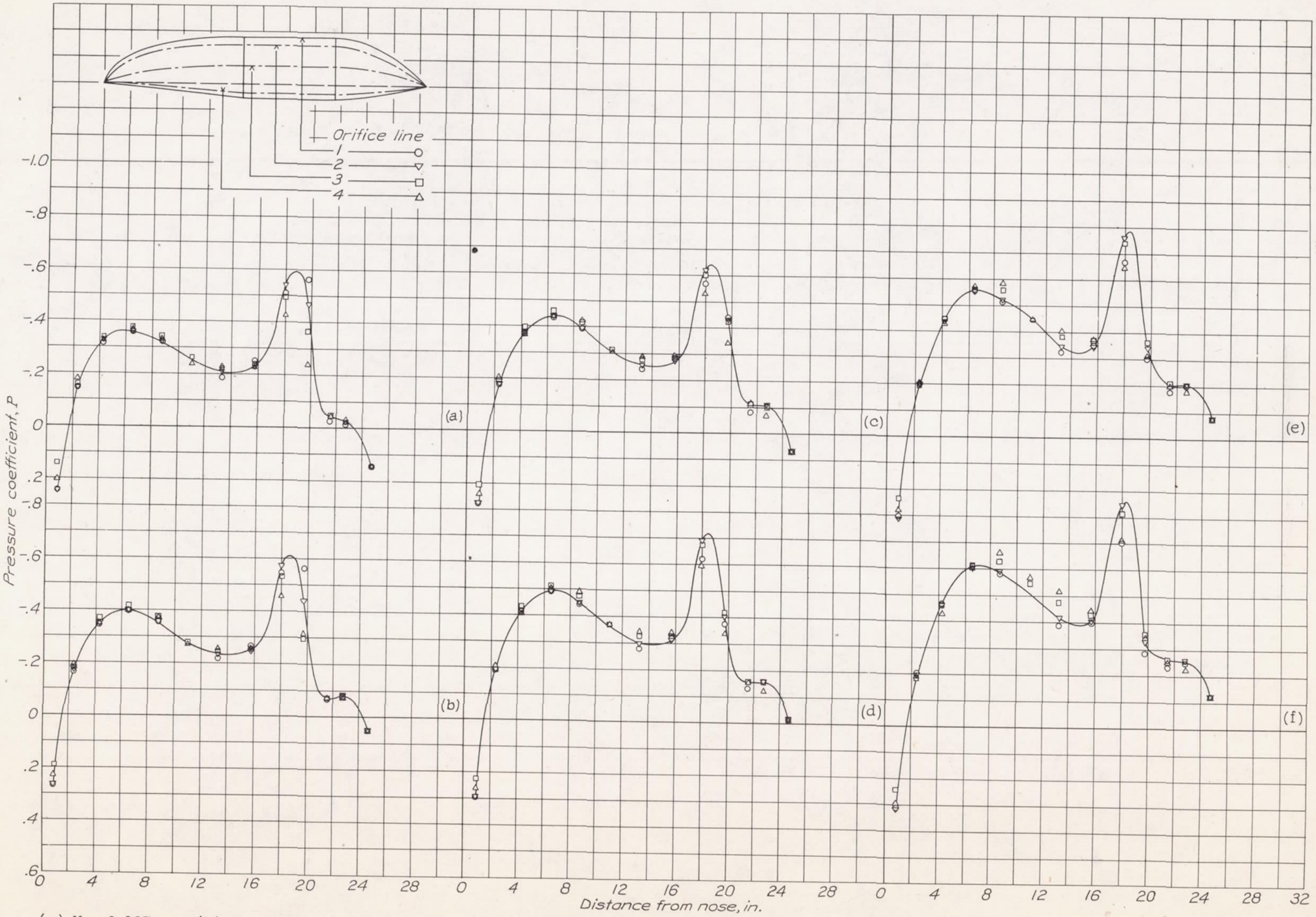

(a) M , 0.197 (b) M , 0.433 (c) M , 0.537 (d) M , 0.627 (e) M , 0.681 (f) M , 0.707

Figure 16.- Pressure distribution about the 3-1-1 windshield for various Mach numbers. α , -0.67°.

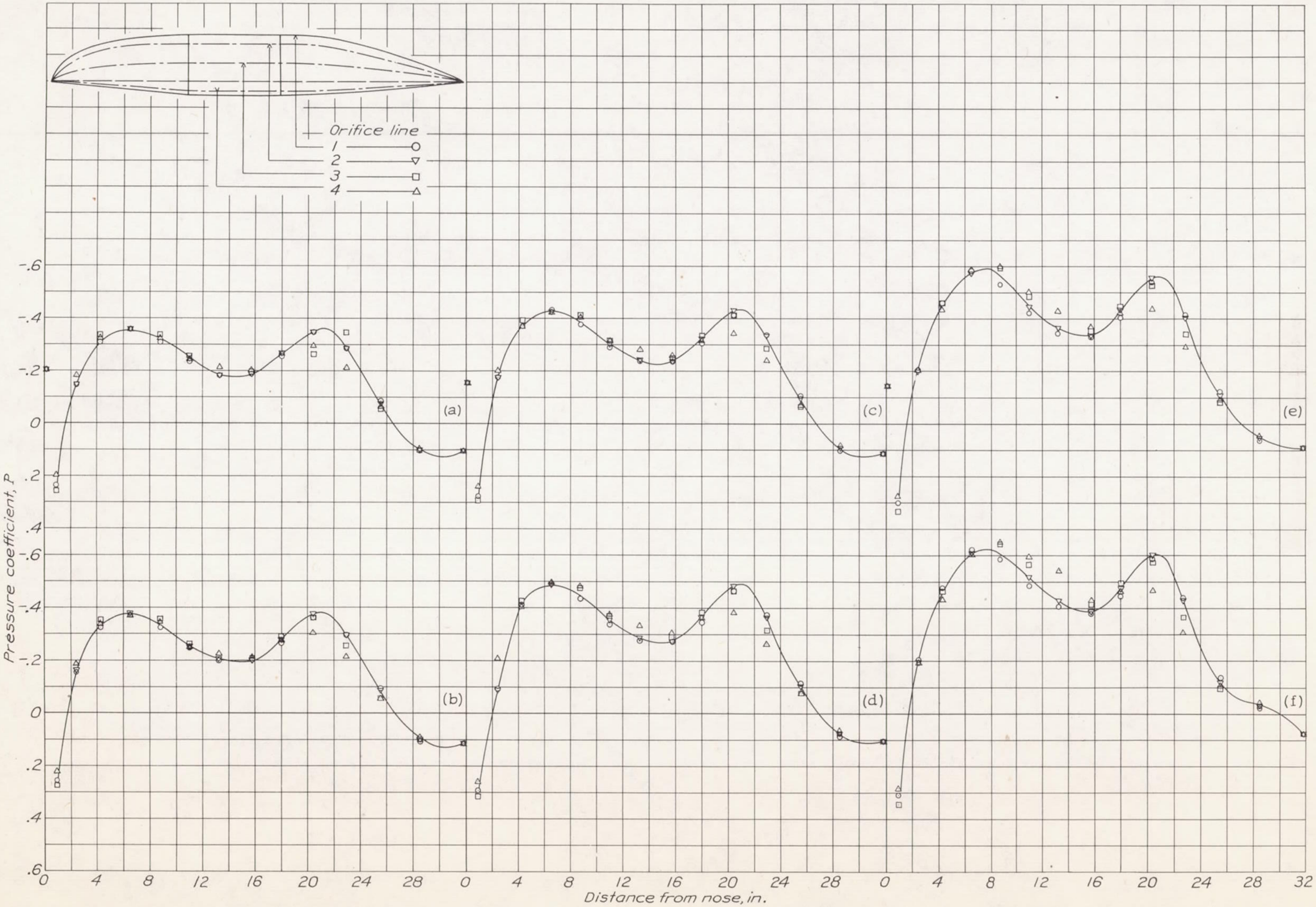

(a) M , 0.195 (b) M , 0.342 (c) M , 0.539 (d) M , 0.630 (e) M 0.692 (f) M , 0.712

Figure 17.- Pressure distribution about the 3-1-2 windshield for various Mach numbers. α , -0.67°.

NACA

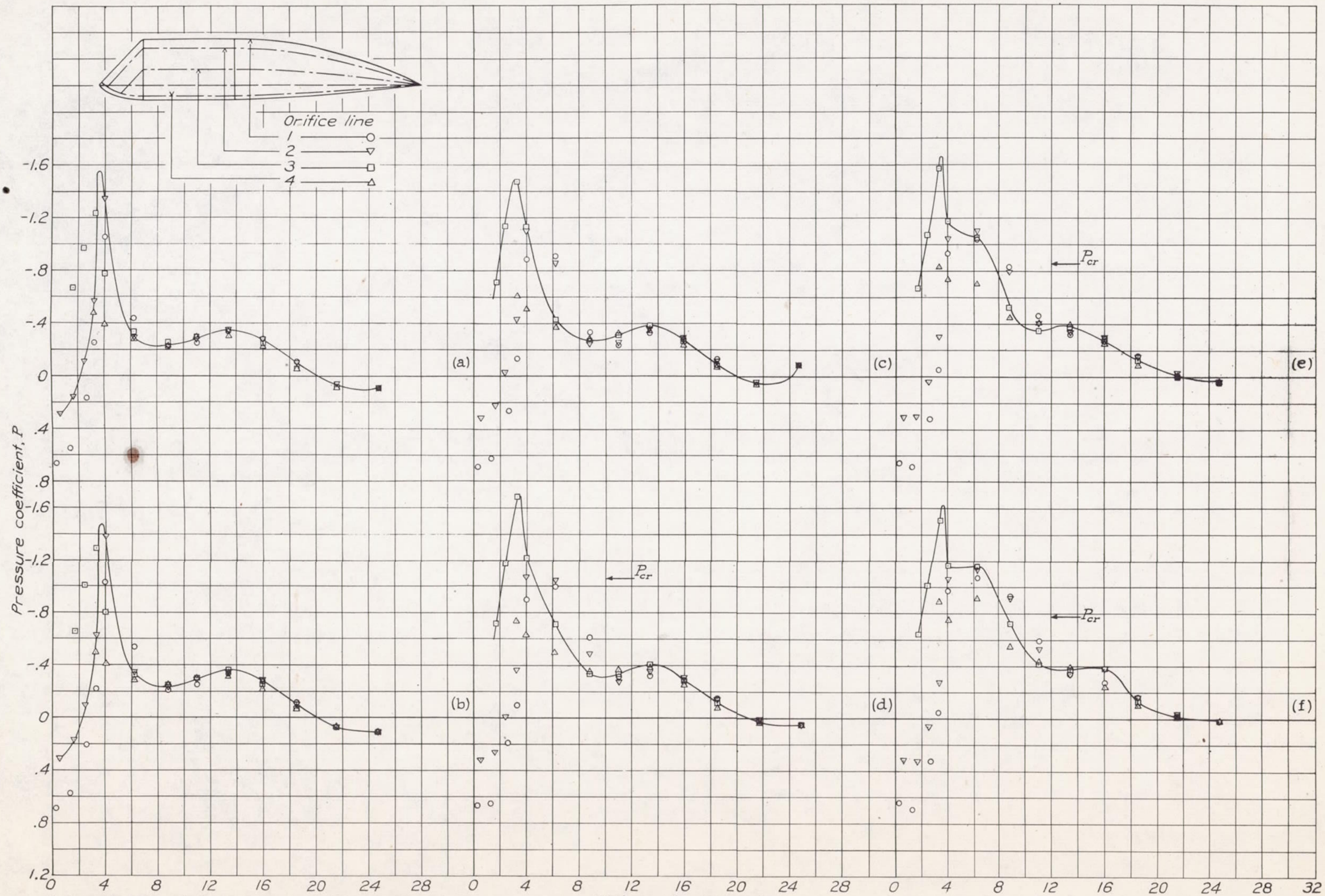

(a) M, 0.192 (b) M, 0.341 (c) M, 0.534 (d) M, 0.637 (e) M, 0.684 (f) M, 0.702

Figure 18.- Pressure distribution about the 6-1-2 windshield for various Mach numbers. α , -0.67°.

Fig. 18

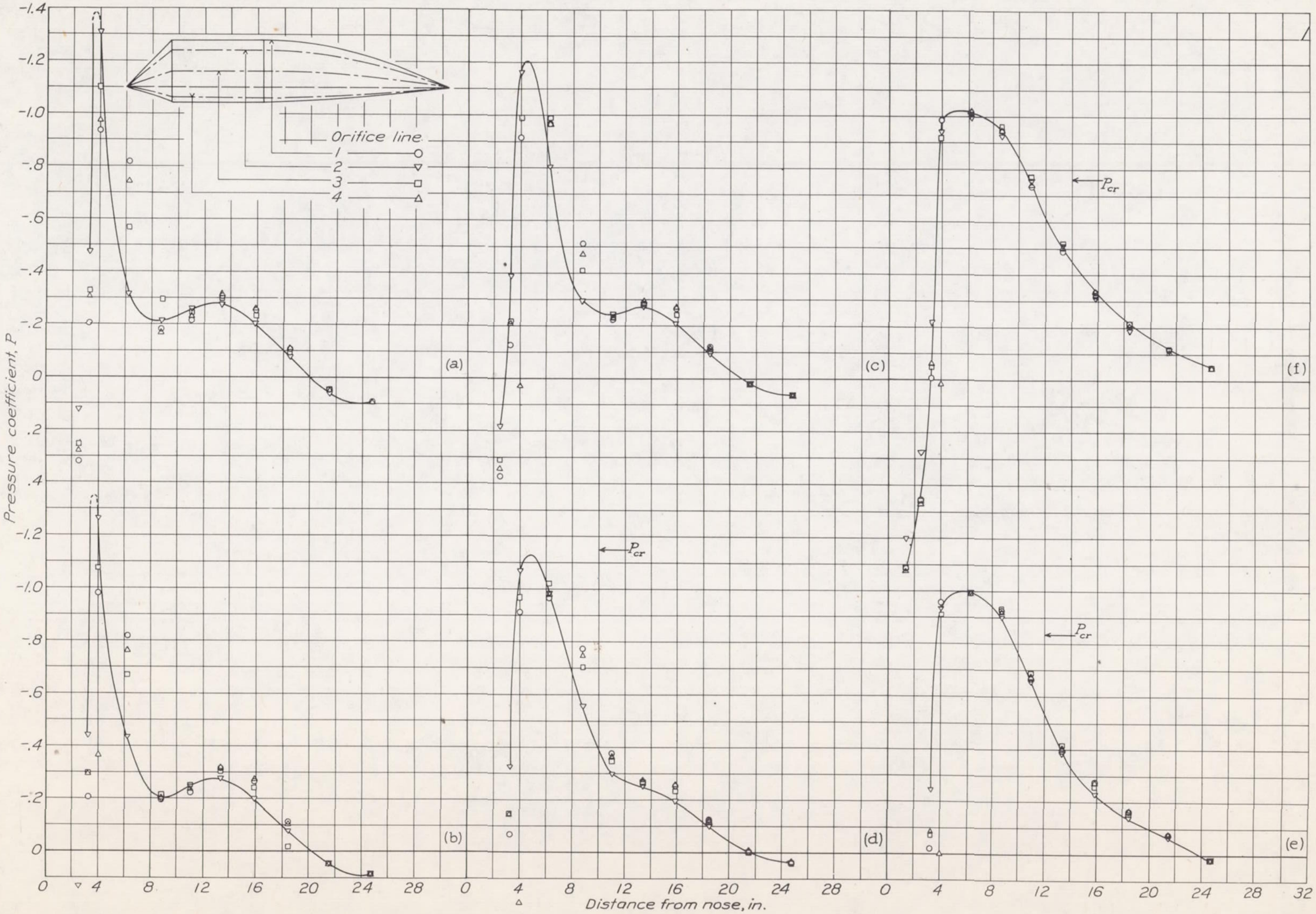

(a) M , 0.196 (b) M , 0.341 (c) M , 0.537 (d) M , 0.627 (f) M , 0.704 (e) M , 0.689

Figure 19.- Pressure distribution about the 9-1-2 windshield for various Mach numbers. α , -0.67°.

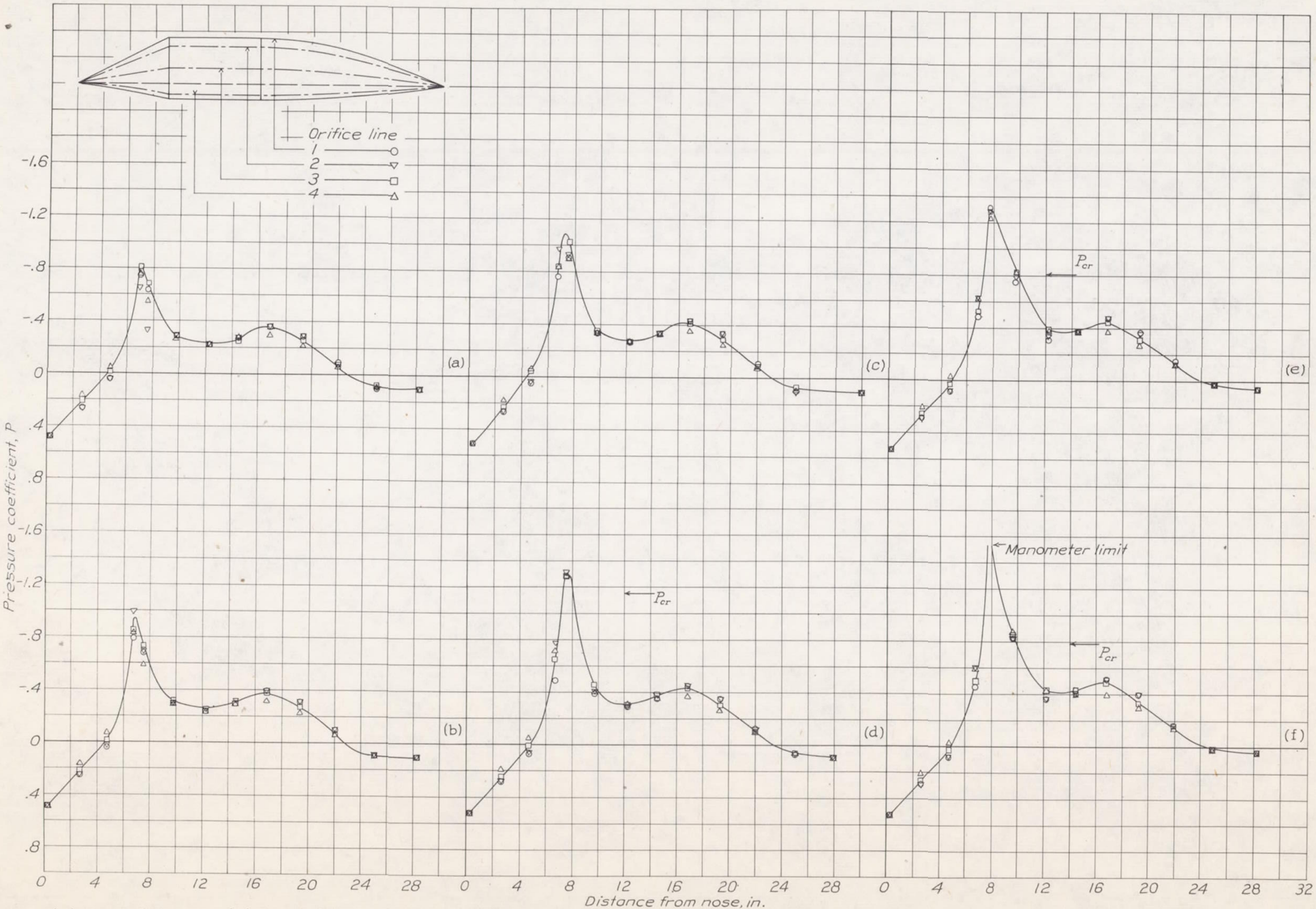

(a) M , 0.190 (b) M , 0.339 (c) M , 0.536 (d) M , 0.626 (e) M , 0.682 (f) M , 0.699

Figure 20.- Pressure distribution about the 10-1-2 windshield for various Mach numbers. α , -0.67°.

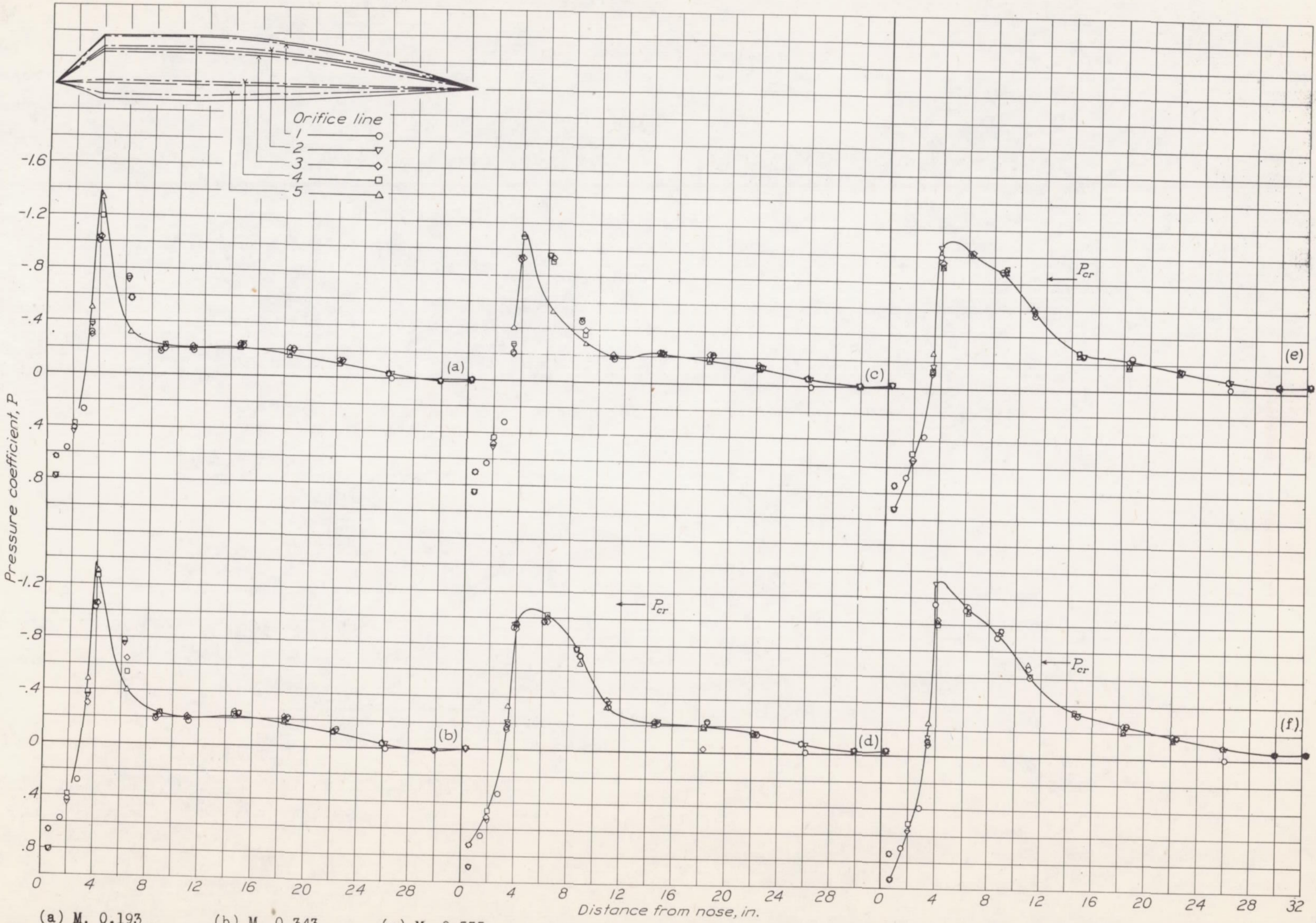

(a) M, 0.193 (b) M, 0.343 (c) M, 0.535 (d) M, 0.633 (e) M, 0.687 (f) M, 0.710

Figure 21.- Pressure distribution about the 7-3-4 windshield for various Mach numbers. α , -0.67°.

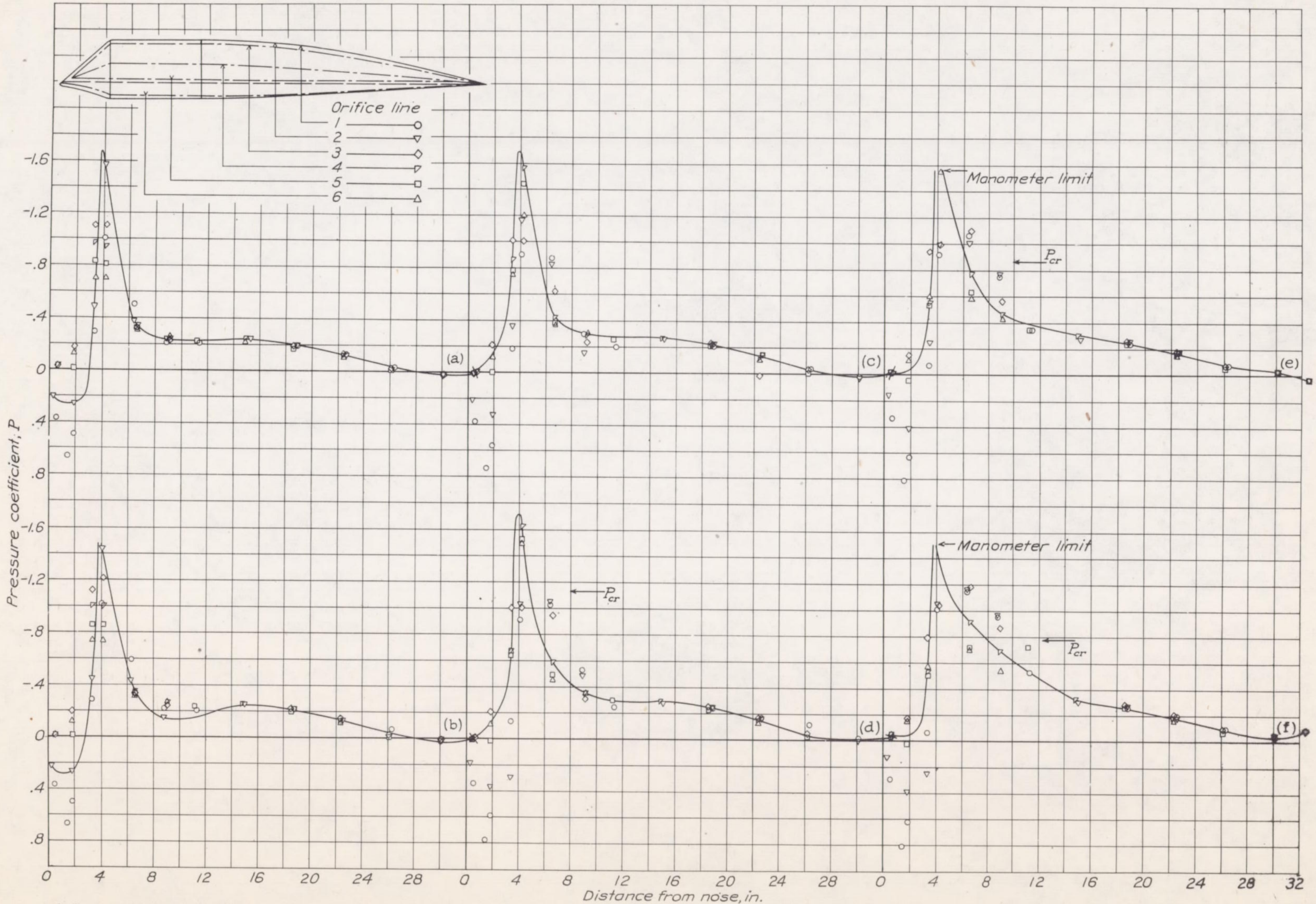

(a) M, 0.192 (b) M, 0.341 (c) M, 0.535 (d) M, 0.631 (e) M, 0.682 (f) M, 0.702

Figure 22.- Pressure distribution about the 8-4-5 windshield for various Mach numbers. α , -0.67°.

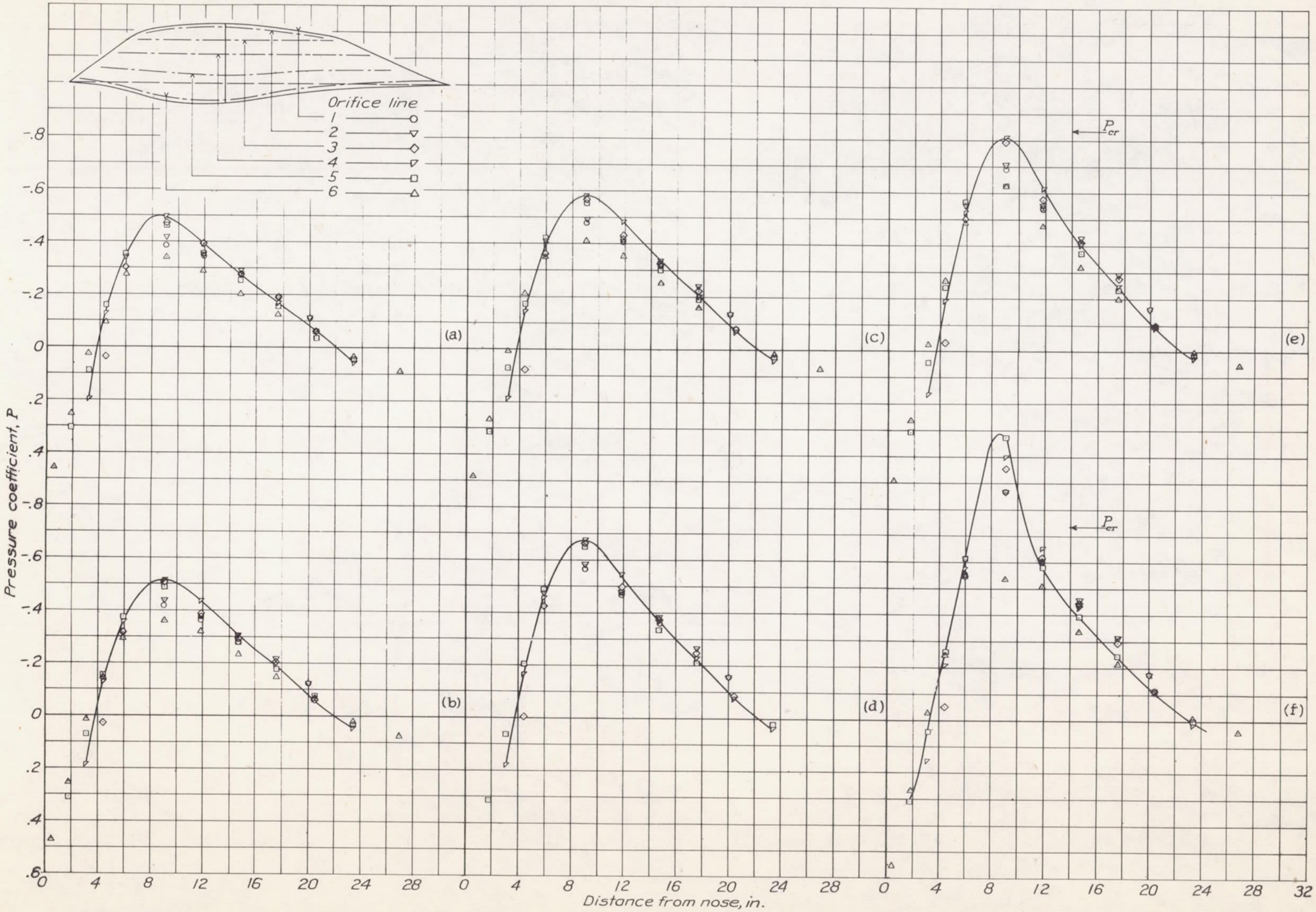

(a) M, 0.191 (b) M, 0.341 (c) M, 0.523 (d) M, 0.630 (e) M, 0.688 (f) M, 0.711

Figure 23.- Pressure distribution about the X-1 windshield for various Mach numbers. α , -0.67°.

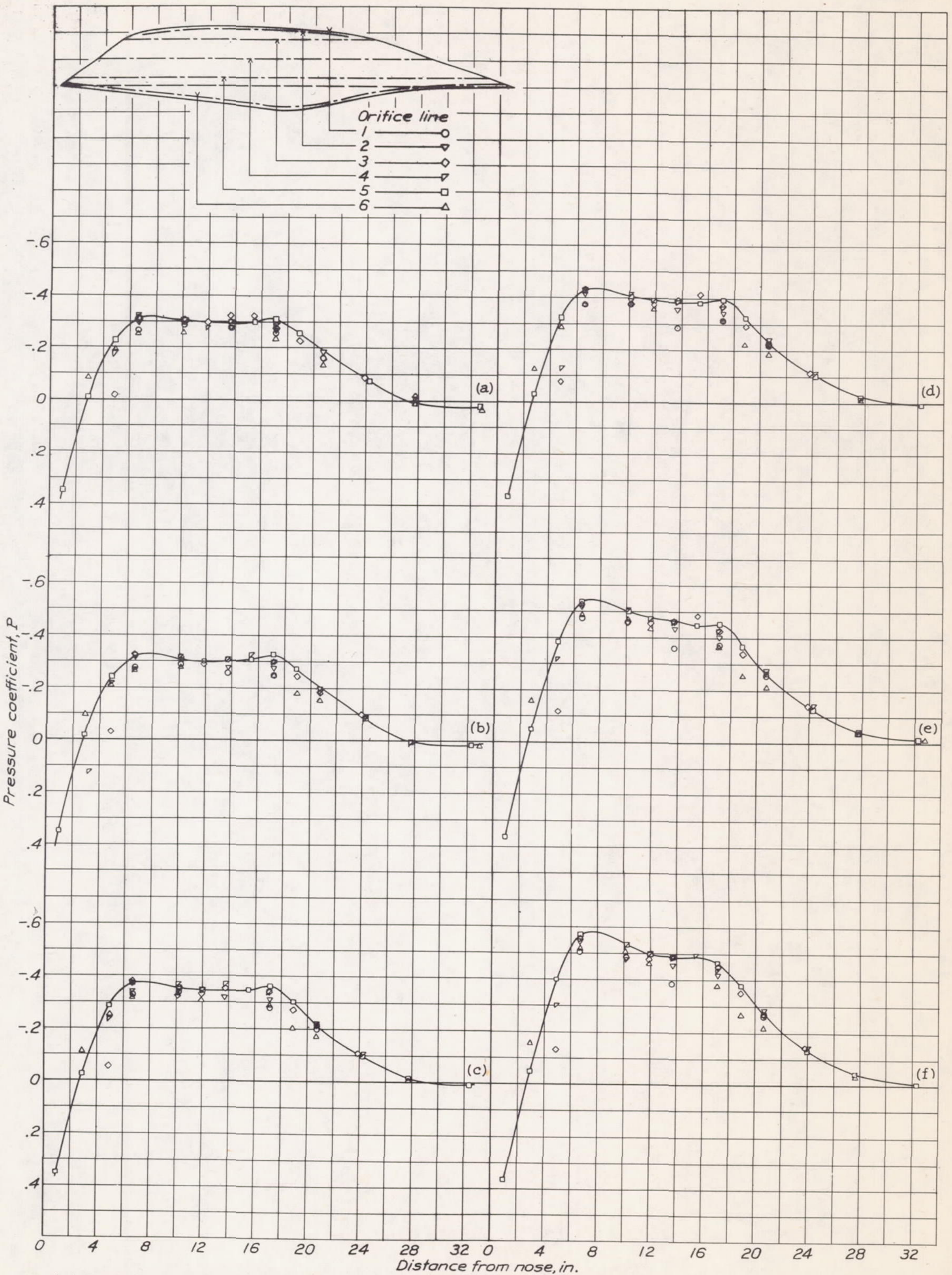

(a) M, 0.194 (b) M, 0.330 (c) M, 0.524 (d) M, 0.623 (e) M, 0.684 (f) M, 0.700

Figure 24.- Pressure distribution about the X-2 windshield for various Mach numbers. α , -0.67°.

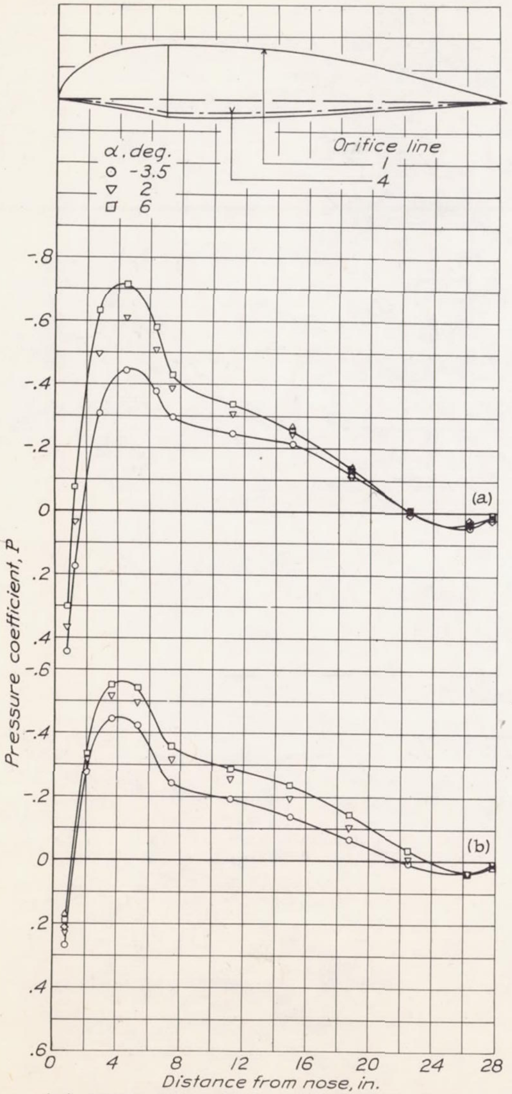

(a) Orifice line 1. (b) Orifice line 4

Figure 25.- Pressure distribution about the 2-0-3 windshield for various angles of attack. M, 0.199.

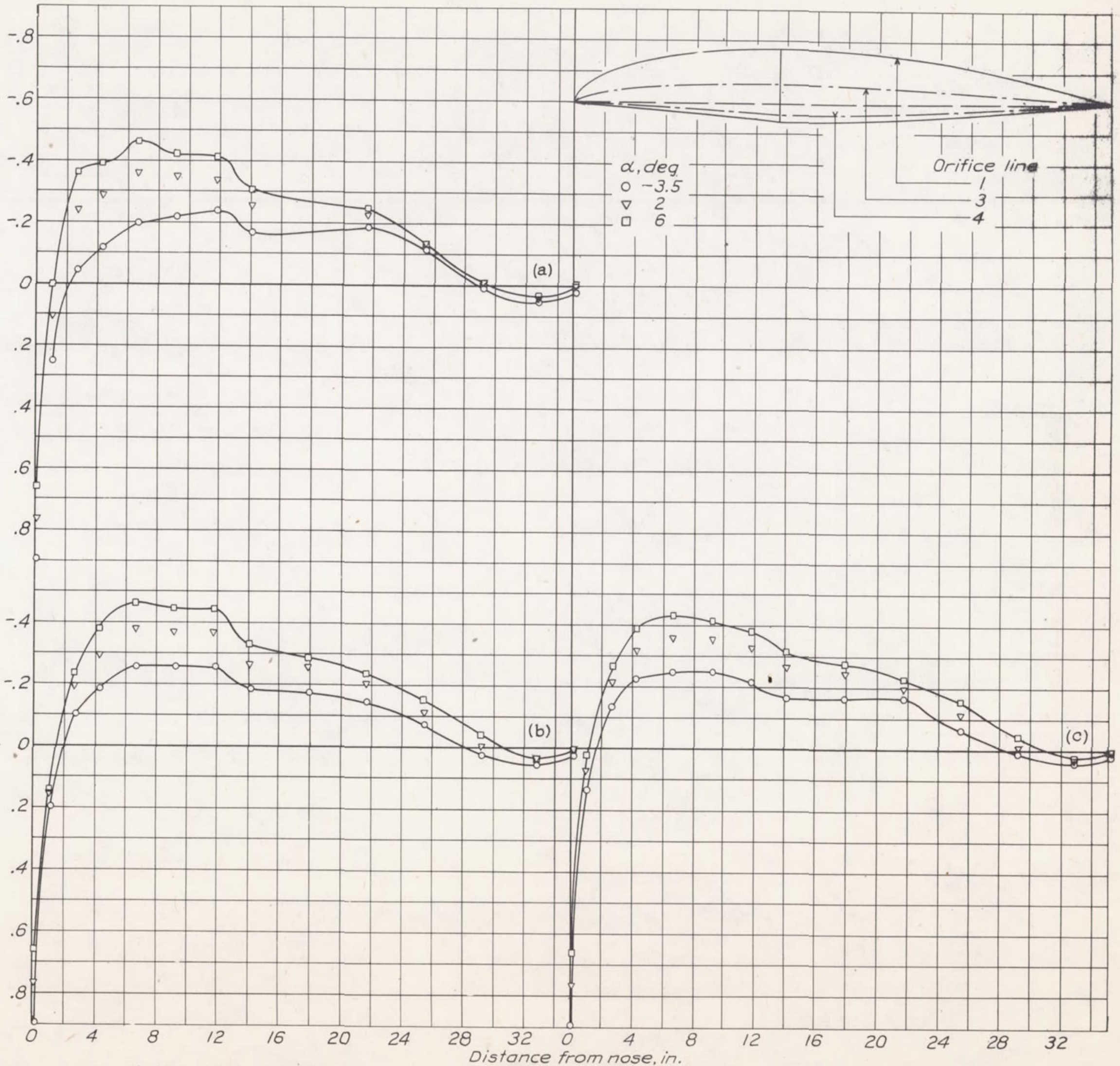

(a) Orifice line 1. (b) Orifice line 3 (c) Orifice line 4

Figure 26.- Pressure distribution about the 4-0-3 windshield for various angles of attack. M, 0.198.

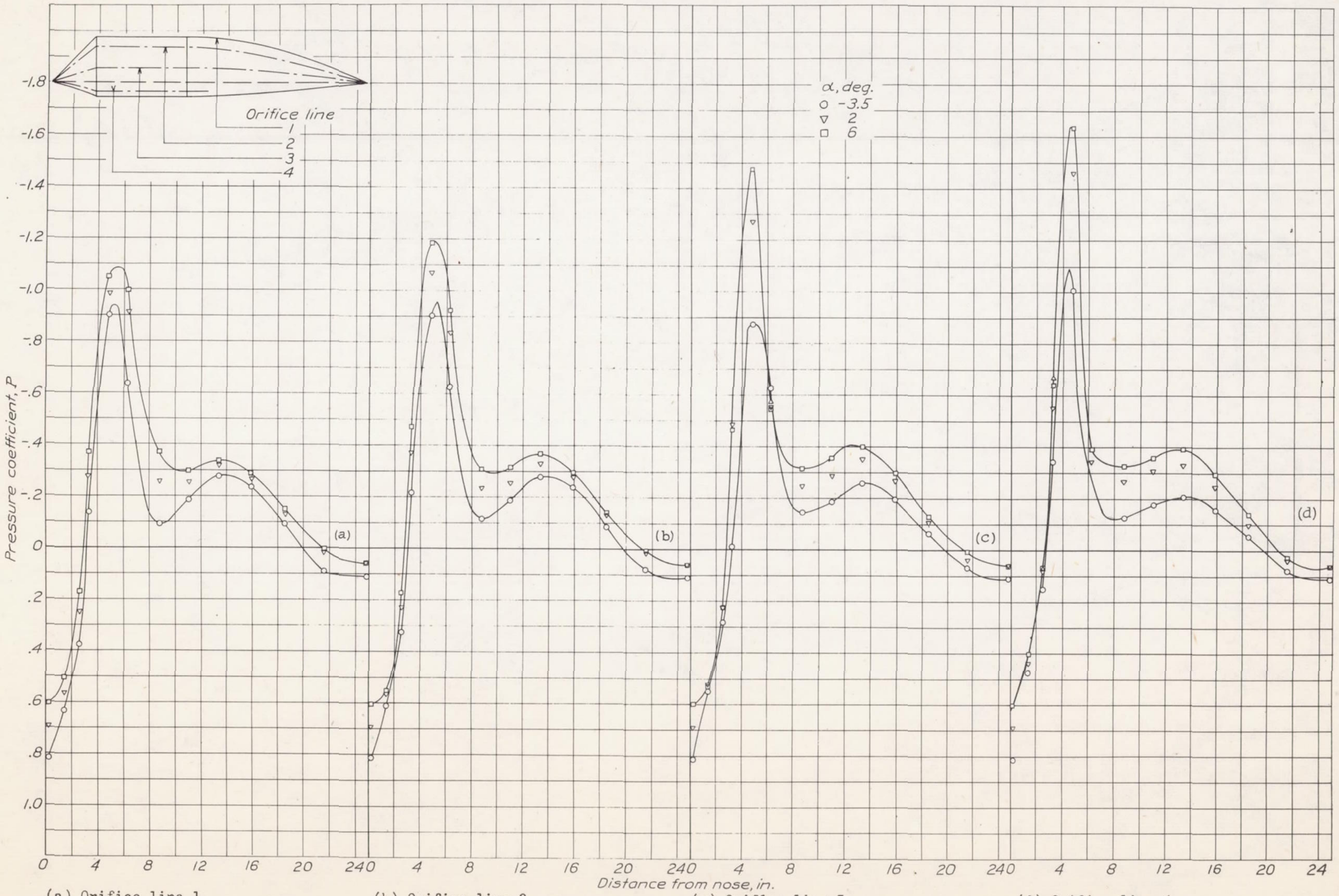

(a) Orifice line 1. (b) Orifice line 2 (c) Orifice line 3 (d) Orifice line 4

Figure 27.- Pressure distribution about the 9-1-2 windshield for various angles of attack. M, 0.196.

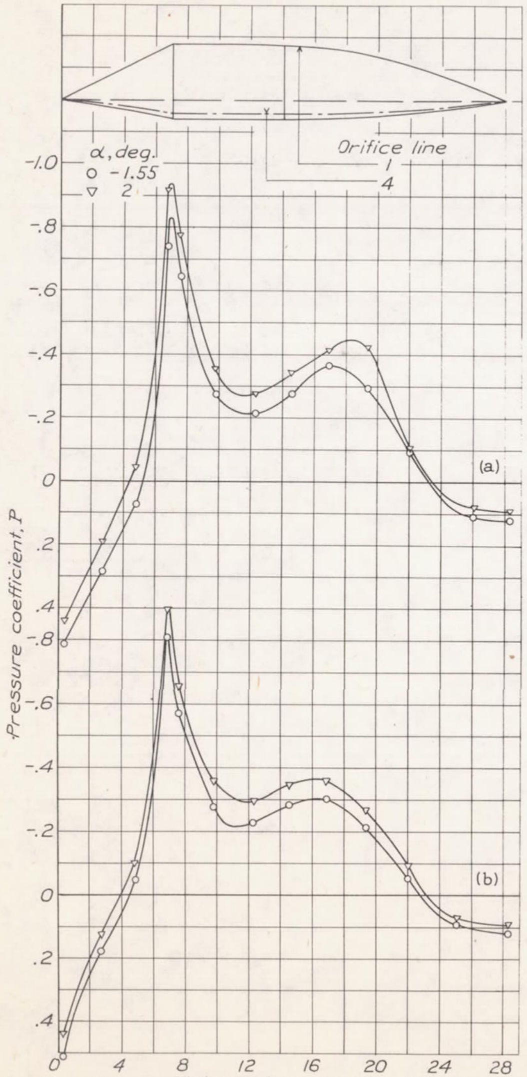

(a) Orifice line 1 (b) Orifice line 4

Figure 28.- Pressure distribution about the 10-1-2 windshield for various angles of attack. M, 0.339.

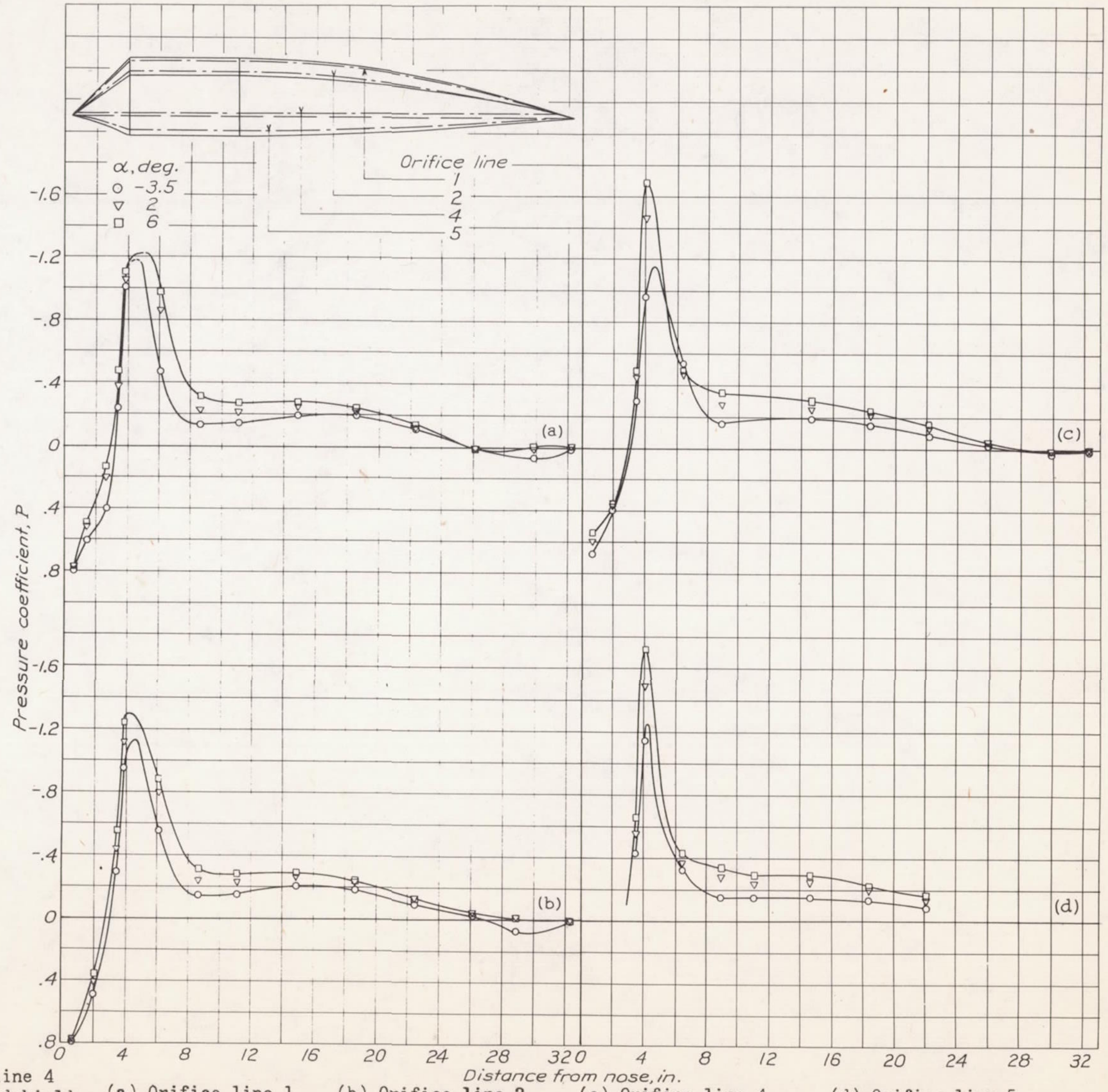

(a) Orifice line 1 (b) Orifice line 2 (c) Orifice line 4 (d) Orifice line 5

Figure 29.- Pressure distribution about the 7-3-4 windshield for various angles of attack. M, 0.192.

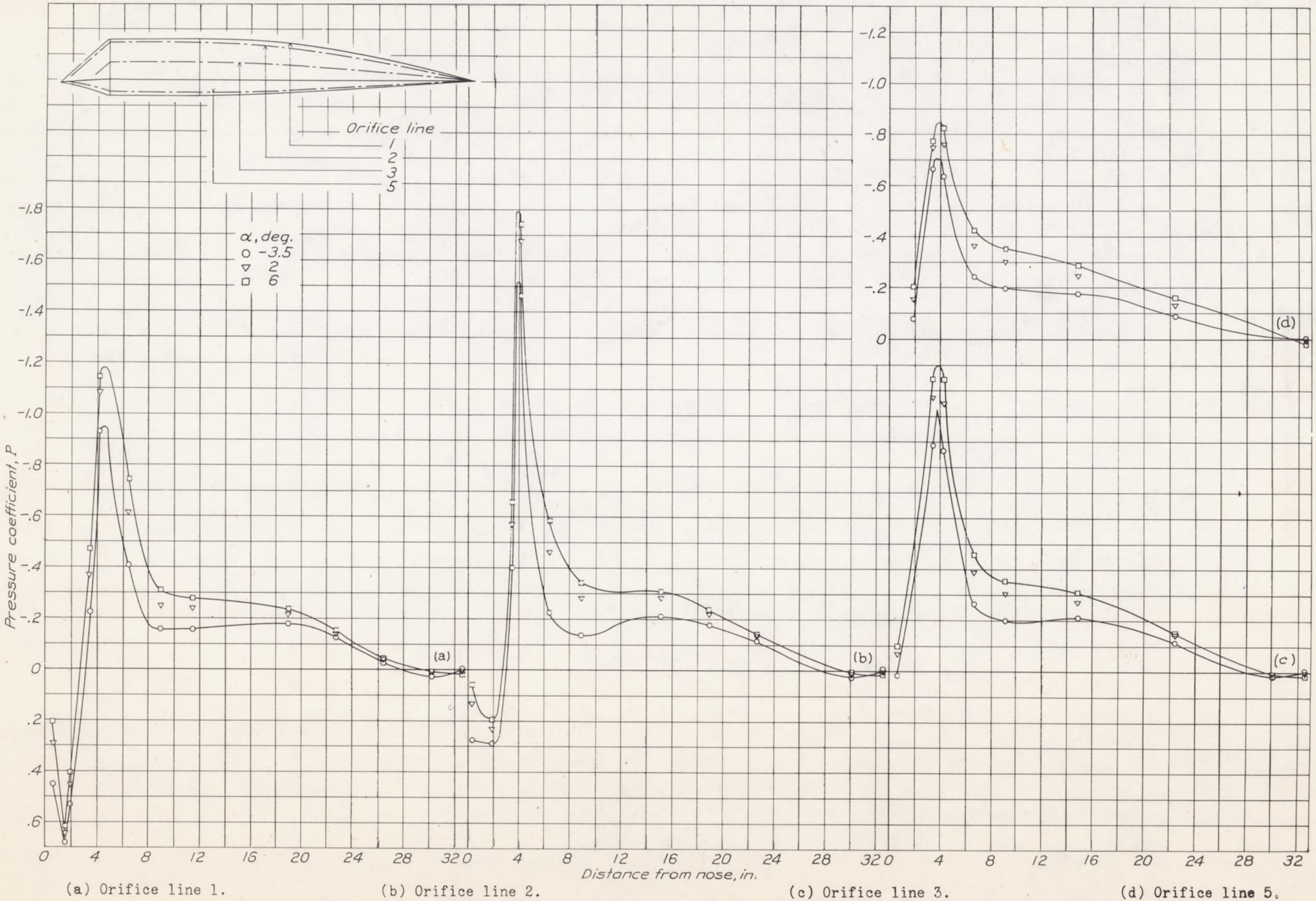

(a) Orifice line 1. (b) Orifice line 2. (c) Orifice line 3. (d) Orifice line 5.

Figure 30.- Pressure distribution about the 8-4-5 windshield for various angles of attack. M, 0.192.

Fig. 30

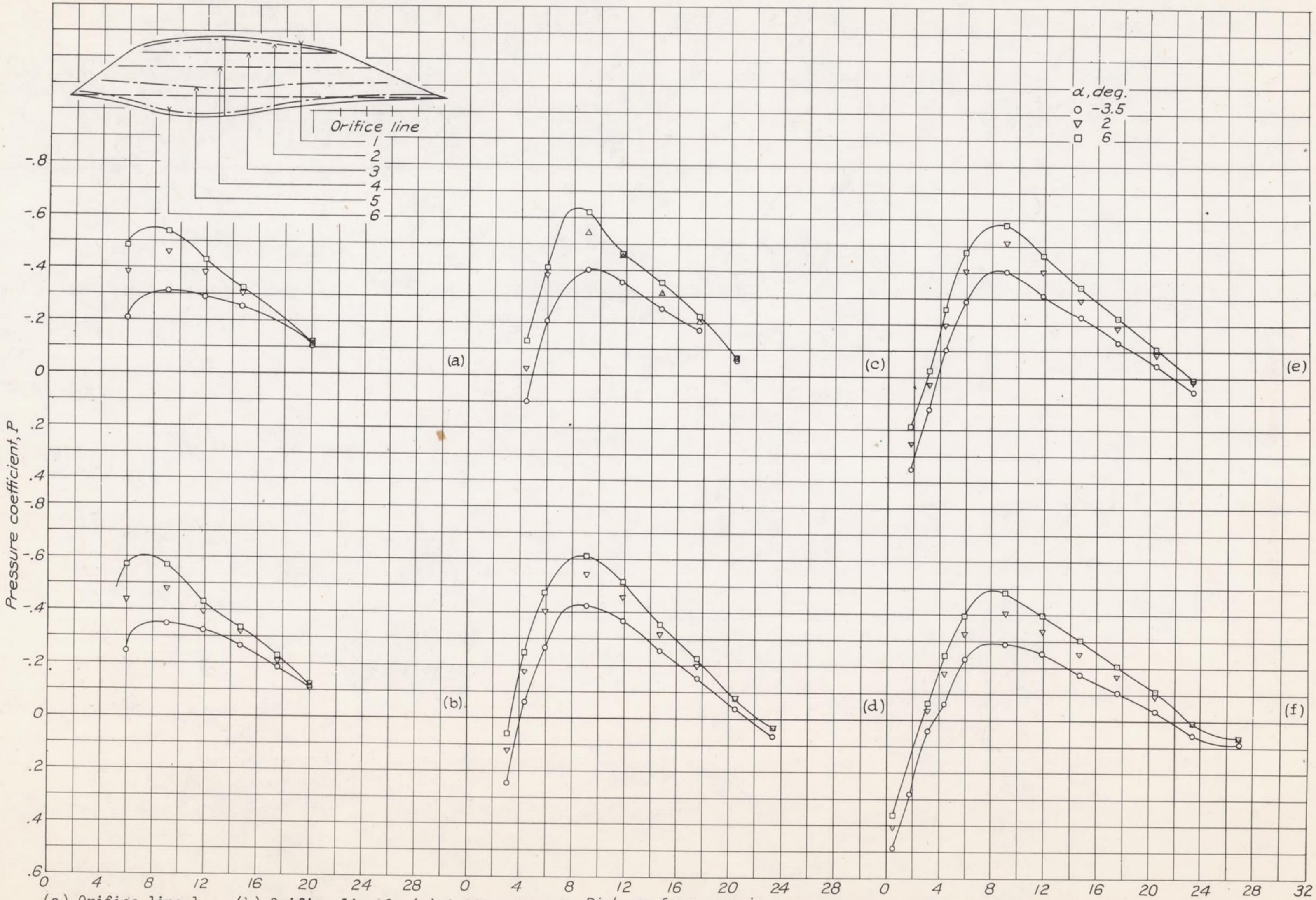

(a) Orifice line 1 (b) Orifice line 2 (c) Orifice line 3 (d) Orifice line 4 (e) Orifice line 5 (f) Orifice line 6

Figure 31.- Pressure distribution about the X-1 windshield for various angles of attack. M, 0.190.

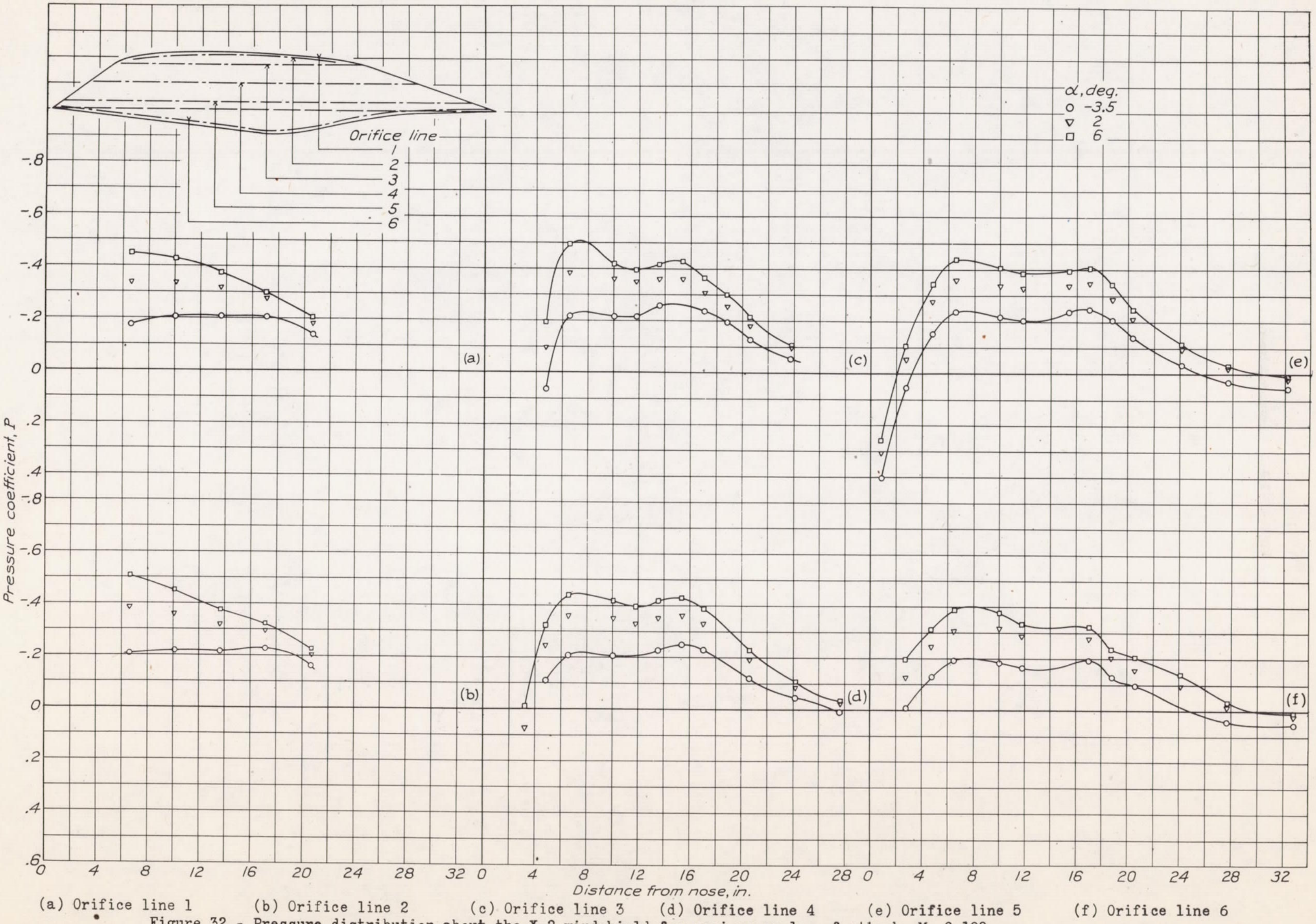

(a) Orifice line 1 (b) Orifice line 2 (c) Orifice line 3 (d) Orifice line 4 (e) Orifice line 5 (f) Orifice line 6

Figure 32.- Pressure distribution about the X-2 windshield for various angles of attack. M, 0.192.

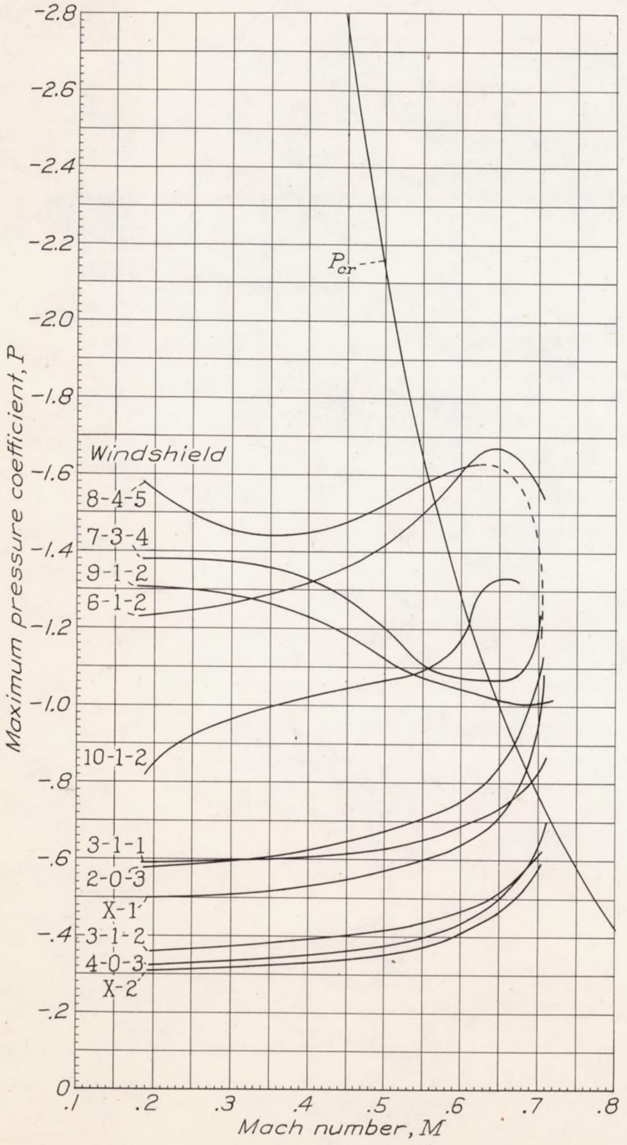

Figure 33.- Variation of the peak negative pressure coefficient with Mach number. α, -0.67°.

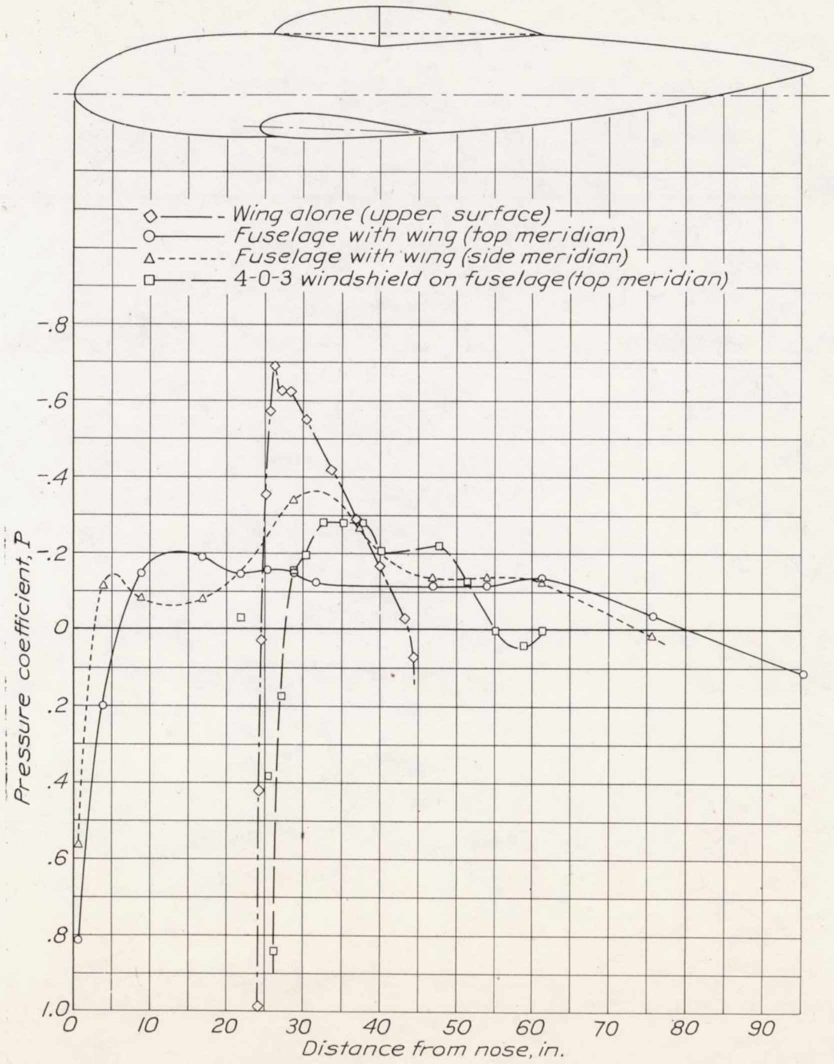

Figure 34.- Pressure distribution on wing, fuselage, and windshield. M, 0.194; α, -0.67°.

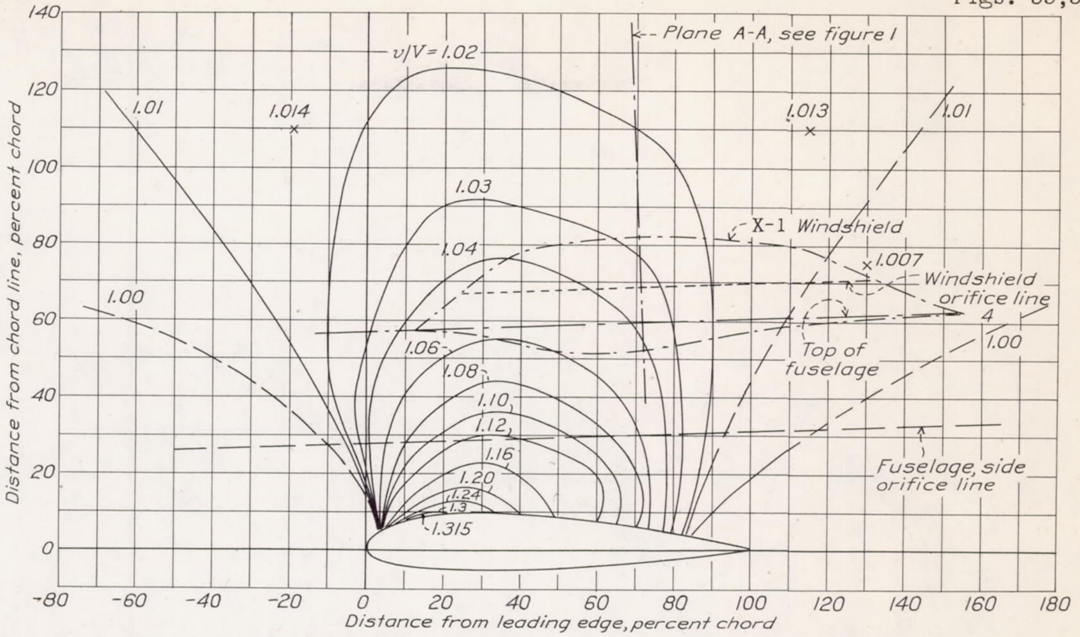

Figure 35.- Theoretical velocity contours for the NACA 2215 wing section. α , -0.67°.

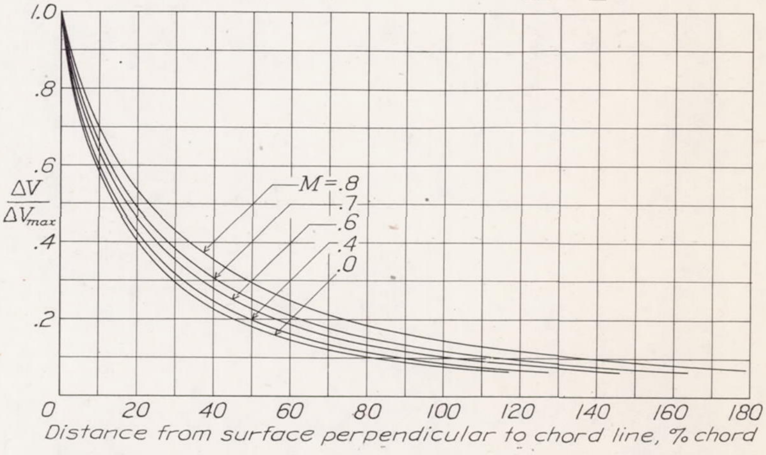

Figure 36.- Decay of velocity increment in field of the NACA 2215 wing.

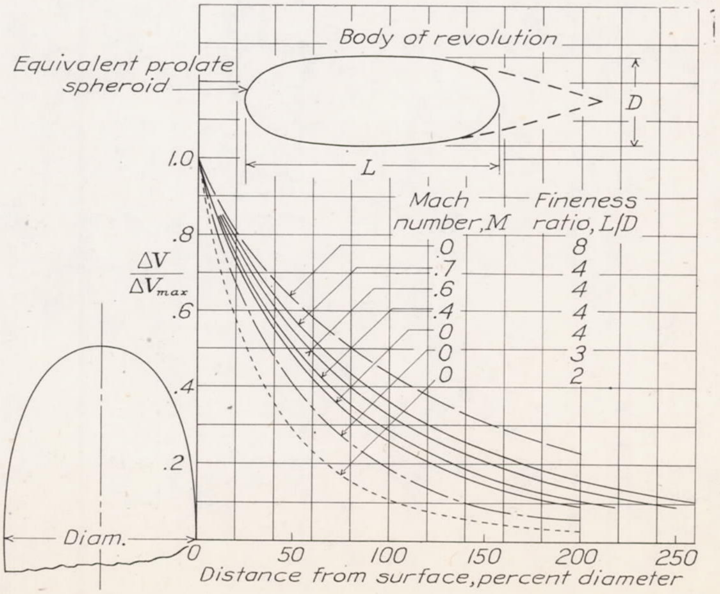

Figure 37.- Decay of velocity increment in field of prolate spheroids.

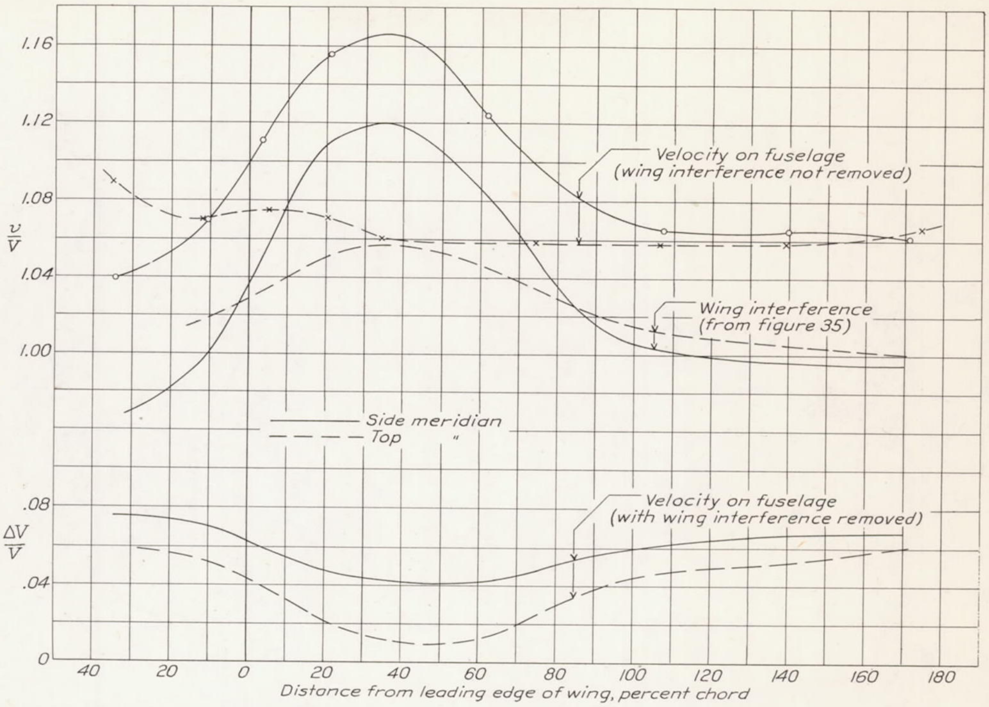

Figure 38.- Correction of velocity distribution on fuselage for wing interference. M , 0.194.

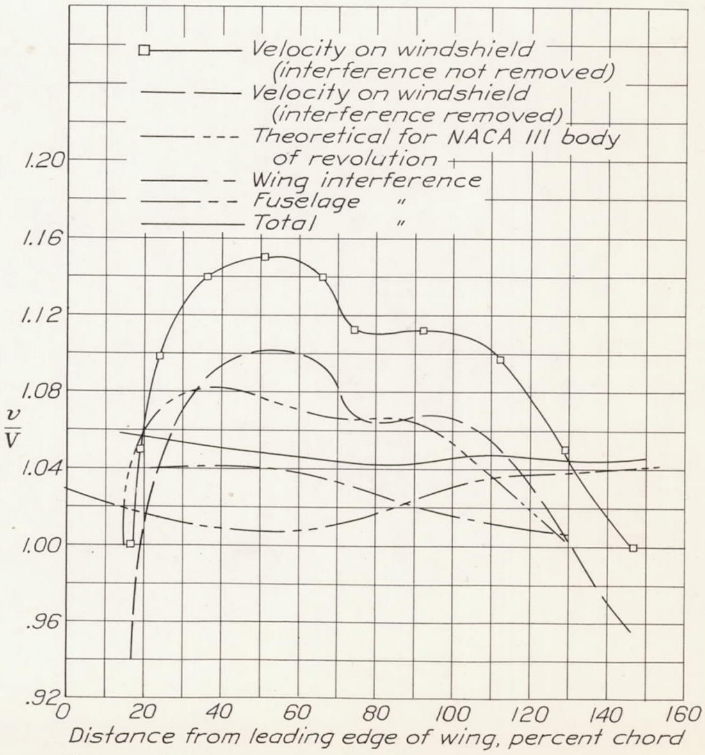

Figure 41.- Correction of velocity distribution on on meridian 3 of 4-0-3 windshield for interference. M , 0.197. α , -0.67°.

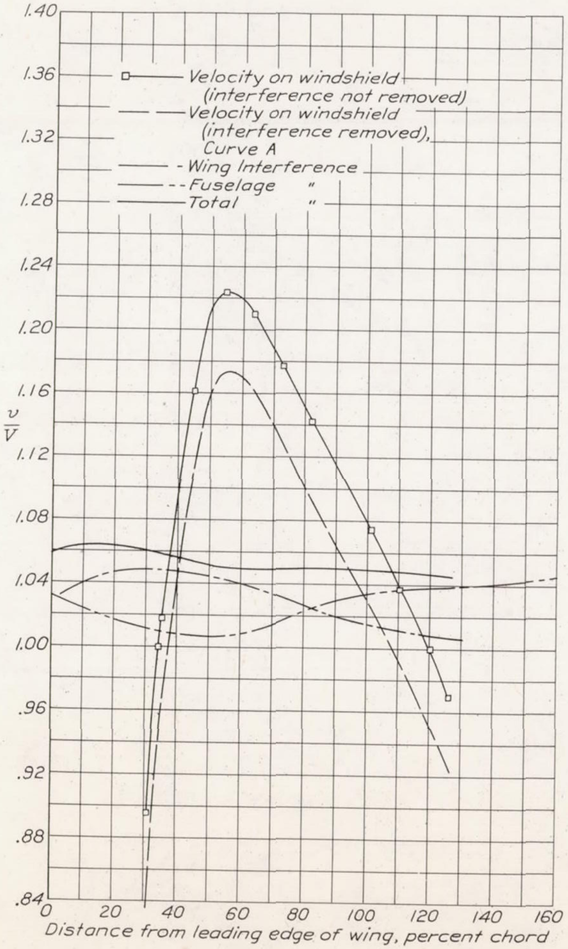

Figure 39.- Correction of velocity distribution on meridian 4 of X-1 windshield for interference. M , 0.191; α , -0.67°.

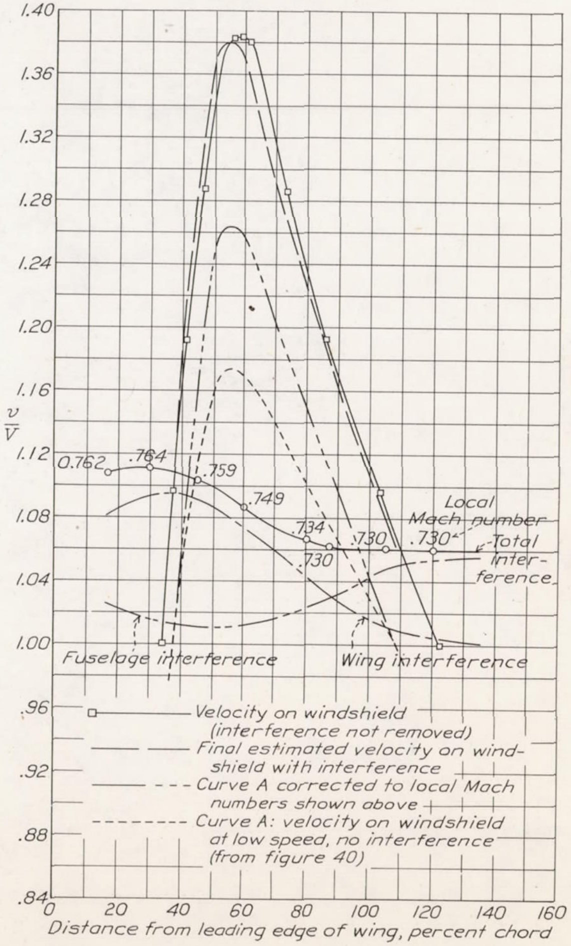

Figure 40.- Correction of velocity distribution on meridian 4 of X-1 windshield for interference. M , 0.688 ; α , -0.67°.